T-3405

# OFFSET AMPLITUDE ANALYSIS OF COMPRESSIONAL SEISMIC DATA FOR FRACTURED RESERVOIR EXPLORATION SILO FIELD, WYOMING

by

Ming-Tar Lu

1988

A thesis submitted to the Faculty and the Board of Trustees of the Colorado School of Mines in partial fulfillment of the requirements for the degree of Doctor of Philosophy (Geophysics).

Golden, Colorado

Date Nov. 23 1988

Signed: Ming-Tar Lu
Ming-Tar Lu

Approved: Thomas L. Davis
Dr. Thomas L. Davis
Thesis Advisor

Golden, Colorado

Date 23 Nov 88

Signed: P R Romig
Dr. Phillip R. Romig
Head, Department of
Geophysics

## ABSTRACT

The Silo field, southeastern Wyoming, produces oil from a naturally-fractured reservoir within the Cretaceous Niobrara Formation. A five-mile P-wave line in this field was processed to preserve amplitude.

P- and S- wave mode conversion and phase velocity variation influence reflectivity changes with offset. Model and seismic data indicate that amplitude decreases in an unfractured zone and increases in a saturated fractured zone of the Niobrara Formation. The amplitude variation with offset is azimuthally dependent on the orientation of the line to the fracture set. P-wave amplitudes analyzed as a function of offset provide another tool for fractured reservoir evaluation.

TABLE OF CONTENTS

TABLE OF CONTENTS
(Continued)

# LIST OF FIGURES

LIST OF FIGURES
(Continued)

# LIST OF PLATES

## ACKNOWLEDGEMENTS

I would like to thank Dr. Thomas L. Davis for his continued guidance, supervision and encouragement throughout this work. Grateful appreciation is extended to the members of my committee, Drs. Frank A. Hadsell, William A. Schneider, John A. DeSanto, Donald I. Dickinson and William M. Barney. I wish to express great appreciation to Dr. Guy Towle for providing facilities and technical advice in core measurements and to the Center for Wave Phenomena for providing software and hardware to simulate the seismic models.

To the following companies, I appreciate the release of the seismic data utilized in the study: Bolt Technology (Kim Tech), CGG American Services, Champlin Petroleum, Conoco, Diamond Shamrock Exploration, Enserch Exploration, Exxon Production Research, Gearhart-Geosource, Intevep, S. A., Mobil Research and Development, Schlumberger Well Services, Standard Oil, and Union Oil of California. I wish to thank CGG American Services for its effort in processing the seismic line. A special thanks goes to Mr. John Young, CGG Processing Supervisor, for his processing expertise.

My graduate program at the Colorado School of Mines was funded by the Chinese Petroleum Corporation. Extra financial aid provided by CGG American Services, Inc., Chevron and Amoco Production Company is most appreciated

I would like to express grateful appreciation to my parents, Lu Guor-Niarn and Chiou Pan-Gueih; my sisters, Jen-Jy, and Jen-Rurng; and my brothers, Ming-Chang and Ming-Tai for their eternal support.

My deepest gratitude is expressed to my wife Lih-Huar and son Cherng for their love, understanding and constant encouragement.

# INTRODUCTION

Seismic P-wave reflection amplitude is a function of P-wave velocity, density, Vp/Vs ratio in each medium, and the angle of incidence. Koefoed (1955) suggested Vp/Vs can be used as an indicator of lithology. Wyllie et al (1961) have shown Vp/Vs can be an indicator of porosity. Pickett (1963) demonstrated Vp/Vs can be an effective diagnostic of rock type. During the early 1970s, bright spot technology began to be used to predict hydrocarbon presence in the subsurface prior to drilling. Investigation started into how seismic reflection amplitudes change in more detail. Ostrander (1984) and Gassaway and Richgels (1983) discussed interpretation of changes in Vp/Vs (or Poisson's ratio) by amplitude offset variation of P-wave reflections. The technique proved especially effective when large changes in Vp/Vs occur, such as those associated with gas-saturated sandstones of high porosity. Domenico (1984), McCormack et al. (1984), Tatham (1982), Dohr and Janle (1980), Hamilton (1979), Gregory (1976), Tatham and Stoffer (1976) have shown the usefulness of combined P-wave and S-wave reflection studies in predicting subsurface lithology.

Crampin et al (1984) indicated that in an azimuthal anisotropic media a S-wave energy splits into two orthogonal shear components propagating each with its own velocity. The time delay between these split S-waves is sensitive to the matrix velocities in the rock (Crampin, 1985). S-wave splitting is caused by internal structure, such as the discontinuity interfaces, but more commonly by anisotropy of the elastic properties of rocks caused by stress-aligned cracks or pores along the wavepath.

Martin (1987) demonstrated that three-component recordings of S-wave can be used to measure azimuthal anisotropy in Silo Field. Two fractured areas were identified within the interval containing the Niobrara Formation, one is NW-SE, the other NE-SW. These measurements yield information of the location, intensity and orientation of subsurface fractures.

Hayden (1984) used P-wave seismic data of reflection amplitude variations and waveform changes to identify fracture development in the subsurface. She showed that wavelet processed, frequency enhanced, normal polarity seismic data and offset modeling are indicative of extensively fractured, hydrocarbon-saturated zones in the Bakken Shale, Antelope field, Williston basin. The critical factors for accurate modeling include variation in the bulk modulus and Poisson's ratio of the rock. The Poisson's ratio is significantly changed for the fractured Bakken, the amplitude of the wave response at large offsets compared to zero offset may be 16 times greater than that for the non-fractured case having a high Poisson's ratio.

Studies have shown that elastic properties of materials such as shale and chalk are anisotropic (Wright, 1987).

The purpose of this study is to analyze P-wave seismic measurement over a naturally fractured reservoir to determine whether fractures can be detected by detailed analysis of the amplitude with offset. Five miles of seismic P-wave data were recorded in Silo field, Wyoming (Figure 1). The field has low permeability and low porosity. Fractures control hydrocarbon production in the Cretaceous Niobrara Formation (Pollastro and Scholle, 1984). Plate I shows a map of wells in the Silo field. The definition of dry hole in Plate I is that the cumulative production is smaller than 1,000 bbl.

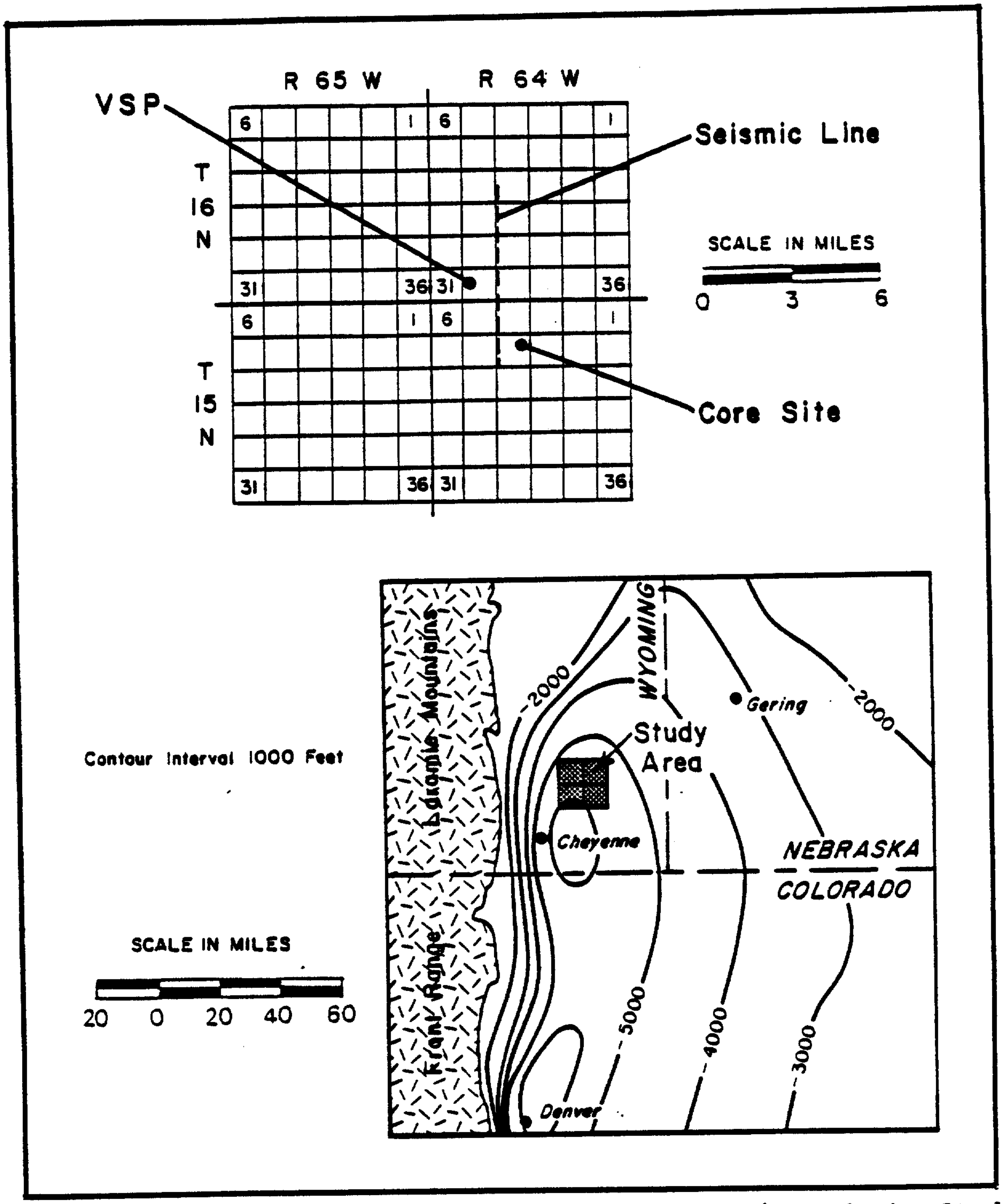


FIGURE 1. LOCATION MAP OF SILO FIELD. Location of the Study Area in the Northern Denver Basin. Mapped Contours are on the Basement. Seismic Line, VSP, and Core Site Shown in Detail Map. (After: Martin, 1987)

## THEORY OF OFFSET AMPLITUDE IN ISOTROPIC MEDIA

Figure 2 illustrates a plane P-wave incident on an isotropic rigid flat interface with horizontal slowness in the direction of increasing x, P-wave incident at angle $i_1$, reflected and transmitted P-waves occur at the boundary at angles $i_1$ and $i_2$ and reflected and transmitted SV-waves at angles $j_1$ and $j_2$, respectively. In terms of the scalar potential Ø for the compressional waves and the vector potential A for the transverse waves, In Region 1. the displacement and stress components are written on the z=0 surface as

$$u_1^{(1)}(x,0) = \frac{\partial\phi^{SC}}{\partial x}(x,0) - \frac{\partial A^{(1)}}{\partial z}(x,0) + \frac{\partial\phi^{in}}{\partial x}(x,0) \quad ,$$

$$u_3^{(1)}(x,0) = \frac{\partial\phi^{SC}}{\partial z}(x,0) + \frac{\partial A^{(1)}}{\partial x}(x,0) + \frac{\partial\phi^{in}}{\partial z}(x,0) \quad ,$$

$$\tau_{z1}^{(1)}(x,0) = \mu_1\left[\frac{\partial^2 A^{(1)}}{\partial x^2}(x,0) - \frac{\partial^2 A^{(1)}}{\partial z^2}(x,0) + 2\,\frac{\partial^2\phi^{SC}}{\partial x\partial z}(x,0)\right]$$
$$+ 2\mu_1\,\frac{\partial^2\phi^{in}}{\partial x\partial z}(x,0) \quad ,$$

and

$$\tau_{z3}^{(1)}(x,0) = 2\mu_1\left[\frac{\partial^2\phi^{SC}}{\partial z^2}(x,0) + \frac{\partial^2 A^{(1)}}{\partial x\partial z}(x,0)\right] - \lambda_1\, k_{L1}^2\phi^{SC}(x,0)$$
$$+ 2\mu_1\,\frac{\partial^2\phi^{in}}{\partial z^2}(x,0) - \lambda_1 k_{L1}^2\phi^{in}(x,0) \quad .$$

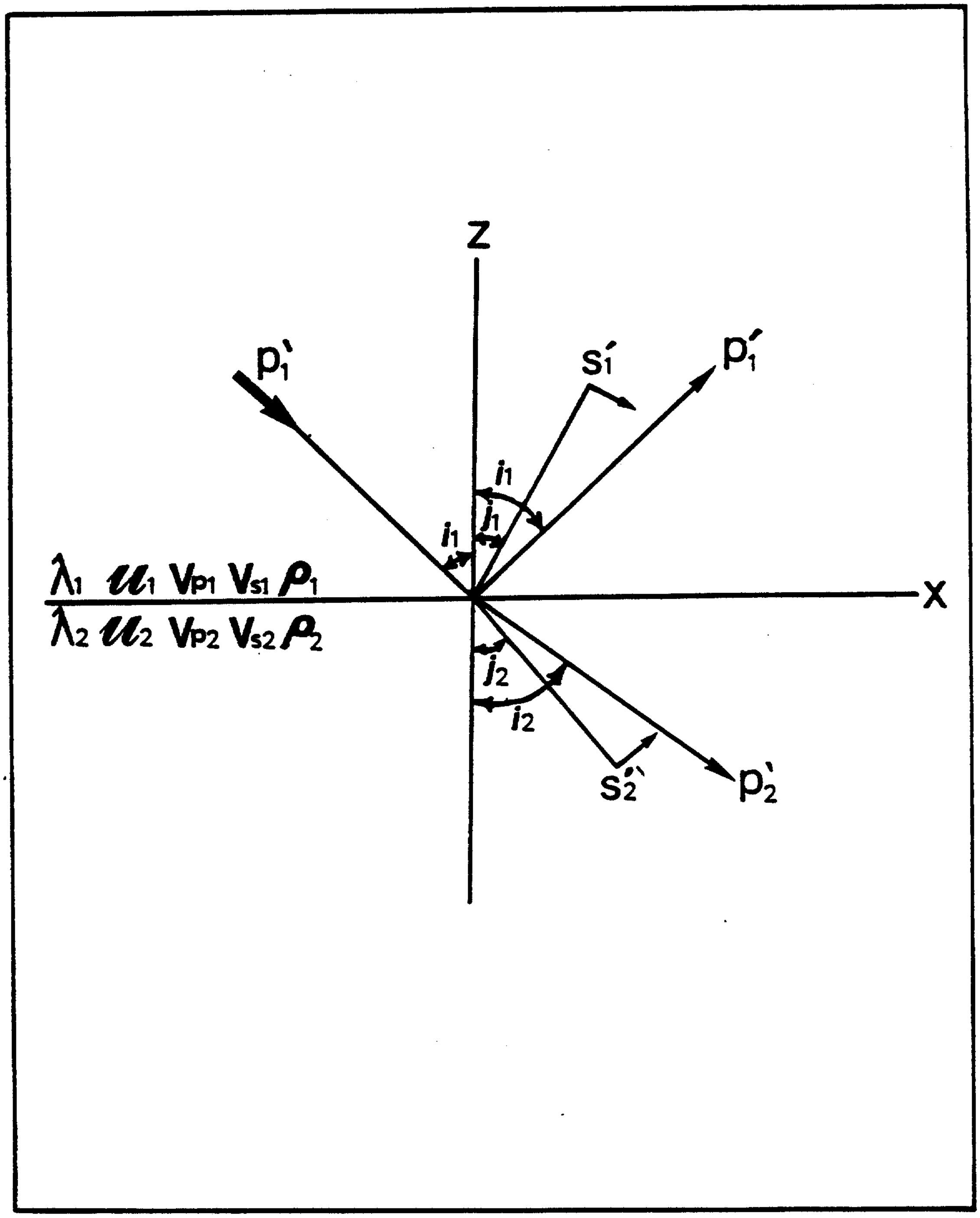


FIGURE 2. REFLECTION AND TRANSMISSION OF P-WAVE INCIDENCE. Diagram of Angular Relations Between Incident, Reflected and Refracted Rays When a P-wave Incident on a Boundary Between Two Different Solid Media.

similarly, the displacement and stress components expressed in terms of these potentials are given by (on the z=0 surface)

$$u_1^{(2)}(x,0) = \frac{\partial}{\partial x}\phi^{(2)}(x,0) - \frac{\partial}{\partial z}A^{(2)}(x,0) \quad ,$$

$$u_3^{(2)}(x,0) = \frac{\partial}{\partial z}\phi^{(2)}(x,0) + \frac{\partial}{\partial x}A^{(2)}(x,0) \quad ,$$

$$\tau_{z1}^{(2)}(x,0) = \mu_2\left[\frac{\partial^2}{\partial x^2}A^{(2)}(x,0) - \frac{\partial^2}{\partial z^2}A^{(2)}(x,0)\right] + 2\mu_2\frac{\partial^2}{\partial x\partial z}\phi^{(2)}(x,0) \quad ,$$

and

$$\tau_{z3}^{(2)}(x,0) = 2\mu_2\left[\frac{\partial^2}{\partial z^2}\phi^{(2)}(x,0) + \frac{\partial^2}{\partial x\partial z}A^{(2)}(x,0)\right] - \lambda_2 k_{L2}^2\phi^{(2)}(x,0) \quad .$$

where $\lambda$, $\mu$ are Lame's constants, $K_L$ is compressional wave number.

The boundary conditions for two elastic media in rigid contact are the continuity of displacements and stresses at the z=0 interface (see DeSanto, 1986, for example).

combine with Snell's law

$$\frac{\sin i_1}{V_{P_1}} = \frac{\sin i_2}{V_{P_2}} = \frac{\sin j_1}{V_{S_1}} = \frac{\sin j_2}{V_{S_2}} = P$$

where p is the ray parameter.

Aki and Richards (1980) normalized the incident P1`=1. The four scattered wave displacement amplitudes are P1´, S1´, P2` and S2`. Zoeppritz equations (modified from Aki and Richards, 1980):

$$\begin{pmatrix} P`P' \\ P`S' \\ P`P` \\ P`S` \end{pmatrix} = \begin{pmatrix} -V_{P1}P & -\cos j_1 & V_{P2}P & \cos j_2 \\ \cos i_1 & -V_{S1}P & \cos i_2 & -V_{S2}P \\ 2\rho_1 V_{S1}^2 P\cos i_1 & \rho_1 V_{S1}(1-2V_{S1}^2P^2) & 2\rho_2 V_{S2}^2 P\cos i_2 & \rho_2 V_{S2}(1-2V_{S2}^2P^2) \\ -\rho_1 V_{P1}(1-2V_{S1}^2P^2) & 2\rho_1 V_{S1}^2 P\cos j_1 & \rho_2 V_{P2}(1-2V_{S2}^2P^2) & -2\rho_2 V_{S2}^2 P\cos j_2 \end{pmatrix}^{-1} * \begin{pmatrix} V_{P1}P \\ \cos i_1 \\ 2\rho_1 V_{S1}^2 P\cos i_1 \\ \rho_1 V_{P1}(1-2V_{S1}^2P^2) \end{pmatrix} \quad \text{.............................. (1)}$$

Zoeppritz equations which give the reflection and transmission coefficients for plane waves as a function of angle of incidence and six independent elastic parameters - three on each side of the reflecting interface, three elastic parameters for each medium are P-wave velocity ($V_p$), S-wave velocity ($V_s$), and density ($\rho$).

Knott's (1899) equation for reflection coefficients and Zoeppritz's (1919) equation are a similar set of relations for displacement amplitude except that the latter is considered as different in direction from that of our diagram by the angle $\pi$. Therefore, Equation (1) has an opposite sign for term P1`. Hales and Roberts (1973) commented that many versions of Zoeppritz equations had sign errors. Aki emphasized that Aki and Richards (1980) formulas for P-wave incident and its reflection amplitude with offset are correct (personal communication, April 1987). Macelwane and Sohon (1936), Waters (1978), Aki and Richards (1980) had equations the same as equation (1) but different signs in the elements. According to different definitions, Nafe (1956) used complex variable methods to calculate reflection coefficients, Richter (1958) had the same signs and elements as Zoeppritz. Young and Braile (1976) produced a computer program for application of Zoeppritz amplitude equations, and all the results are the same as that of Aki and Richards (1980).

# WAVE PROPAGATION IN ANISOTROPIC MEDIA

Over the last decade a number of developments for wave motion in anisotropic media have been published in the geophysical literature. However, anisotropy is a rather common phenomenon and may be caused by a variety of mechanisms including crystal alignments, lithological alignments, stress-induced effects, thin layers and most commonly, two-phase materials and aligned cracks. The assumption in the analysis for anisotropy is that the wavelengths of the seismic signal are greater than the layer thickness, because anisotropic effects are greatest in areas where the layering is quite thin (10-50 ft) (Berryman, 1979). Therefore, under this assumption any material displaying variations of properties with respect to direction are limited to the variations of anisotropic symmetry systems and can be modelled wholly consistent with the purely elastic wave motion.

Based on the theoretical developments introduced by Crampin (1984), five basic relationships can be derived, which may be found in any textbook of theoretical elasticity (see Love, 1944, for example). For a plane wave propagating in the $x_1$-direction with phase velocity c, the general expression for this homogeneous plane wave is

$$u_j = a_j \exp [iw(t-x_1/c)] \qquad (2)$$

where a is the amplitude vector specifying the polarization of the particle motion. Substituting the displacement equation 2 into the equation of motion, $\rho \ddot{u}_j = C_{j\kappa mn} u_{m,n\kappa}$ where ($\rho$) is density, ($\mu_j$) is the component of displacement in the jth direction, $\{c_{j\kappa mn}\}$ is the fourth-order tensor of elastic constants and $\{u_{m,n\kappa} = \partial u^2 m/\partial x_n \partial X_\kappa\}$, gives three simultaneous equations as a linear eigenvalue problem for $\rho c^2$.

$$(T - \rho c^2 I)\ a = 0 \qquad (3)$$

where T is the 3 x 3 matrix, the eigenvalue problem equation 3 has three real positive roots for ($\rho c^2$) with orthogonal eigenvectors a. These roots refer to a quasi P-wave (qp) and two quasi shear waves (qs1 and qs2), where <u>quasi</u> indicates that these waves have only superficial resemblance to the isotropic P and S-wave.

For any wave propagating in an anisotropic medium, there are three body-waves propagating with velocities varying with direction and with polarization dependent on the particular symmetry system. Therefore in anisotropic propagation, the solutions of equation 3 tracing out three velocity surfaces. But in isotropic media, the isotropic elastic tensor is invariant with rotation and

$$T = \begin{pmatrix} \lambda+2\mu & 0 & 0 \\ 0 & \mu & 0 \\ 0 & 0 & \mu \end{pmatrix}$$

The well-known isotropic velocities can be written down

$$C = \alpha = \sqrt{\frac{\lambda+2\mu}{\rho}}$$

for the compressional P-wave velocity and the repeated roots

$$C = \beta = \sqrt{\frac{\mu}{\rho}}$$

for the shear wave velocities.

After present consistent theoretical formulations for the numerical solution of a number of wave propagation in anisotropic media, Crampin (1981) concluded that the solution of most problems in anisotropic propagation can be formulated, if the corresponding solution exists for isotropic propagation, and may be solved at the cost of considerably more numerical computation.

# PREVIOUS WORK

## Amplitude with Offset

Muskat and Meres (1940) published reflection coefficients with Poisson's ratio $\sigma_1 = \sigma_2 = 0.25$, Where $\sigma_1$ is the Poisson's ratio of medium 1 and $\sigma_2$ is Poisson's ratio of medium 2. Koefoed (1955) extended the work of Muskat and Meres by hand calculation of Zoeppritz equations for different Poisson's ratios and velocities. He recognized the impact of Poisson's ratios on amplitude variations and predicted the usefulness in predicting lithology from seismic observations. Bortfeld (1962) derived the approximation formulas for reflection coefficients of the P-wave as follows:

$$A_{RP} = \frac{1}{2} \ln \left( \frac{V_{p(n+1)}\ \rho_{(n+1)}\ \cos i_n}{V_{pn}\ \rho_n\ \cos i_{(n+1)}} \right) + \left(\frac{\sin i_n}{V_{pn}}\right)^2 \left(V_{sn}^2 - V_{s(n+1)}^2\right) \left[ 2 + \frac{\ln\left(\dfrac{\rho_{(n+1)}}{\rho_n}\right)}{\ln\left(\dfrac{V_{p(n+1)}}{V_{pn}}\right) - \ln\left(\dfrac{V_{p(n+1)}\ V_{sn}}{V_{pn}\ V_{s(n+1)}}\right)} \right] \quad \text{...... (4)}$$

The equation is satisfactory in an isotropic media up to the critical angle and facilitates insight into the influence of rock properties on reflection amplitudes. Figure 3 is an example of reflection coefficients versus offset on the top of Niobrara calculated from Zoeppritz equations and Bortfeld approximation.

Ostrander (1982) formally introduced amplitude variations with offset to distinguish between gas-generated and nongas-generated amplitude anomalies. For moderate angles of incidence, the relative change in reflection coefficient is particularly significant when the Poisson's ratio difference between the two media is large. Gassaway and Richgels (1983) illustrated how a crossplot of P-wave velocity and Poisson's ratio could be used to estimate gross lithologic variations. Once lithology has been determined, formations containing gas may be recognized from amplitude variations. Shuey (1985) assumed $\Delta Vp/_{Vp}$, $\Delta Vs/_{Vs}$ and $\Delta\rho/\rho$ are all small compared to unity, and simplified Zoeppritz equations by the concatenation of all approximations to arrive at a reflection coefficient

$$R = R_o\ (1 + A\sin^2 i)$$

where $R_o$ is the reflection coefficient at normal incidence. A is a parameter derived from variation of physical properties. This formula approximately accounts for relations between reflection coefficient and elastic

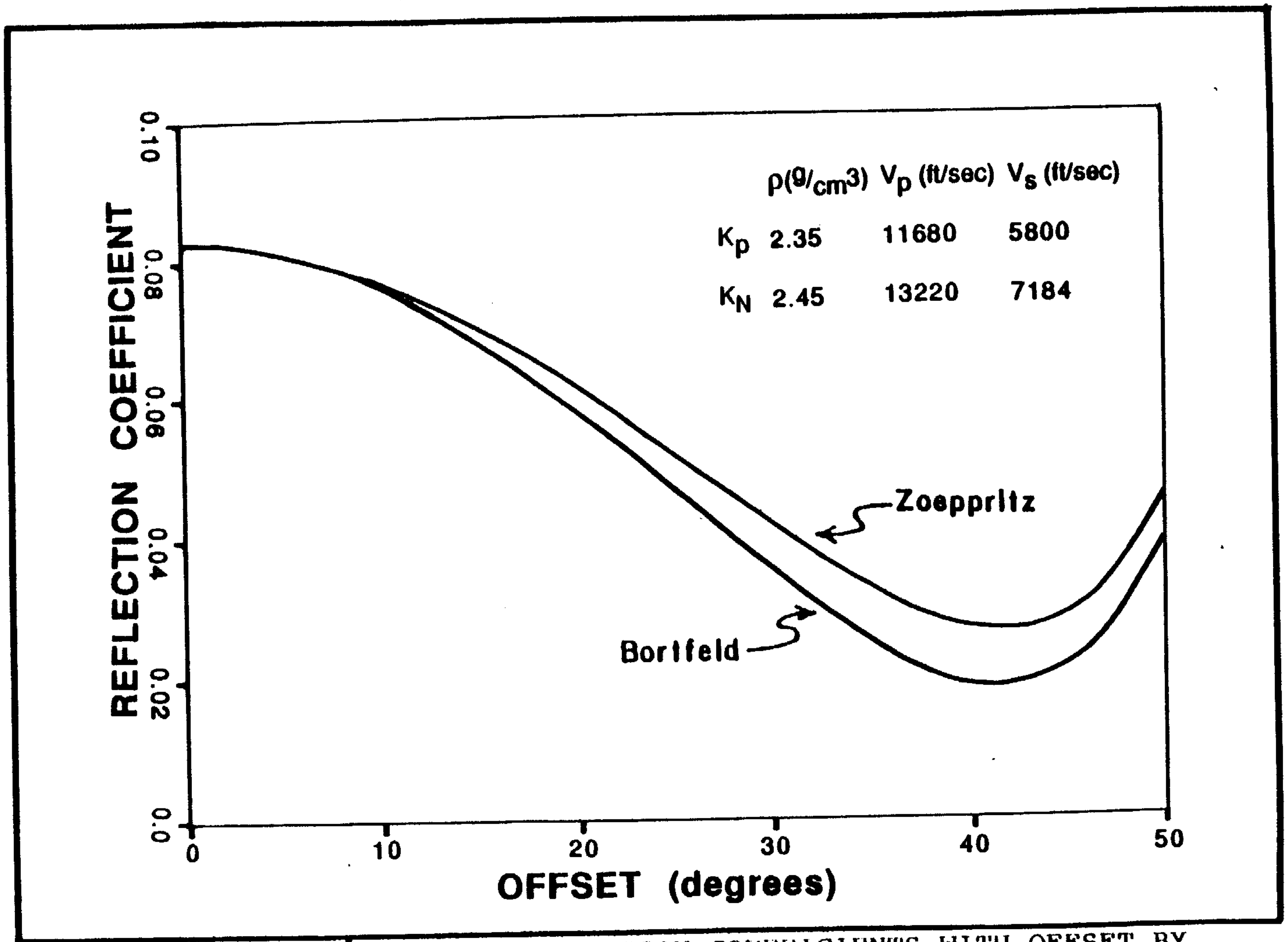


FIGURE 3. COMPARISON OF REFLECTION COEFFICIENTS WITH OFFSET BY ZOEPPRITZ AND BORTFELD EQUATIONS. Reflection Coefficient Versus Offset on the Top of Niobrara (Refer to Diagram of Model), Calculated from Zoeppritz Equations and Bortfeld Approximation.

properties described by Koefoed (1955) in an isotropic medium. Gassaway and Richgels (1986) examined pitfalls in the interpretation of seismic amplitude with offset. They emphasized modeling and attention to detail in data processing.

## Lithologic Properties Indicator

Pickett (1963) indicated the distinct difference in Vp/Vs for limestone, dolomite and clean sandstone, and popularized the use of the Vp/Vs as a lithology indicator. Poisson's ratio can be expressed in terms of P-wave and S-wave velocities:

$$\sigma = \frac{(Vp/Vs)^2 - 2}{2[(Vp/Vs)^2 - 1]}$$

Therefore, Vp/Vs and Poisson's ratio could be used interchangeably. In this study, Poisson's ratio will be the principal interpretation quantity rather than using Vp/Vs ratio. For many sedimentary rocks, a close relationship exists between velocity and density (Gardner, 1974) so that a density contrast across a discontinuity closely follows a velocity contrast across the same interface.

P-wave velocity alone may not be sufficient to identify the cause of velocity anomalies. However, S-wave velocity is less sensitive to the fluid saturant than the P-wave velocity, therefore, it can be used as a normalized quantity with which to compare P-wave velocity. Erickson, et al (1968) proposed that variations in Vp/Vs could be used to identify lateral variation in lithology. Equation 4 shows S-wave energy concentrated in the far trace range (non-normal incidence).

O'Connell and Budiansky (1974) demonstrated P-wave and S-wave velocity behavior variations under certain pressure regimes and different degrees of fracturing and saturation. Results obtained by King (1966), Tatham and Stoffa (1976), and Gregory (1977) showed that fractures should cause an observable increase in the Vp/Vs ratio with the addition of hydrocarbons to the fractures since S-wave velocity is only affected by a small change in the density, and density is reduced by fractures. Gregory (1976) showed that for a pore system filled with oil at a pressure between 1,000 to 5,000 psi, the P-wave velocity increased slightly, but the S-wave velocity decreased even more greatly, therefore, a fractured rock filled with oil (or water) could cause an increasing Vp/Vs ratio. The Vp/Vs ratio could increase in a fractured medium due to the presence of water or oil in the fractures and sufficient fracture density. S-wave velocities were more strongly affected than the corresponding P-wave by a fluid-filled fractured interval. Fracture induced anisotropy produces a variation in the propagation velocity and polarization of seismic waves. For vertically fractured media P-waves at near normal incidence behave as if rocks were isotropic. At near normal incidence S-waves would contain more information about fracture induced anisotropy. Levin (1979) demonstrated anisotropic effects on the shape of normal moveout curves. Anisotropic factors can be deduced in subsurface layers by observation of variations in the reflection amplitude of P-waves with offset. The primary controlling mechanism for Vp/Vs variation in the Niobrara Formation of this study is the fracture density. This observation is supported by the production rate (Figure 9).

## Seismic Anisotropy

The theory of wave propagation in transversely isotropic media is well understood. Many authors including Postma (1955), Gassmann (1964) have presented results dealing with travel-time methods in anisotropic media; in particular, transversely isotropic media. However, kinematic properties alone are not enough to interpret seismic records. Daley and Hron (1977) considered reflection and transmission coefficients of dynamic properties producing a need for synthetic seismograms. White (1982) calculated synthetic seismograms for both compressional and shear-wave propagation in transversely isotropic media by integrating over analytical expressions. White et al. (1983) conducted experimental work to measure the five elastic coefficients which characterize a transversely isotropic medium for the Pierre Shale.

The propagation of seismic body waves in an anisotropic media has been discussed by Crampin (1977). The three body waves (qP, qS1 and qS2) propagating in three-dimensional polarization in anisotropic media, with different velocities, group propagation different from phase - both in velocity and direction - and orthogonal polarization which is not in general coincident with the dynamic axes. Effects of wave propagation in anisotropic media may be subtle and difficult to distinguish from isotropic propagation. The most diagnostic of these effects is the coupling with P and S motion which may be sensitive even to weak anisotropy. Elastic properties must be calculated numerically by using the full elastic tensor or a complicated function of direction cosines.

Although anisotropy effects in geological formations have been extensively documented in the past (Love 1944, White 1955), the development of seismic anisotropy is rapidly evolving in the last ten years (Crampin 1982, Thomsen et al. 1986, Martin 1987 and others). They have shown that microcracking of a rock results in anisotropy of elastic properties which affects wave propagation, the main characteristic is referred to as "shear wave birefringence." O'Connell and Budiansky (1974) described a technique for investigating randomly oriented cracks by plotting Vp/Vs ratio against the Vs velocity. In a transversely isotropic case, if P- and S-wave vertical velocities have a constant relationship with their own horizontal velocities, $V_{13}$ can be estimated from $A_{13} = 2\sigma\ (A_{11}-A_{66})$, where $A_{ij}$ specifies elastic parameters $C_{ij}$ of the medium divided by the density of the medium, $\sigma$ is Poisson's ratio (Wright, 1987). If only the $A_{13}$ of the medium changes, it will control the position of the critical angle, and p-wave reflection will show enormous effects. Considering P-wave effect for the case of transversely isotropic medium, with a horizontal velocity 20% higher than the vertical P-velocity and the horizontal velocity higher in the first layer than the second one, the P-P reflection from the base of the first layer decreases with offset, reversing the trend expected under isotropic conditions.

# GEOLOGY OF SILO FIELD

## Location of Study

Silo field is located in the north-central Denver Basin, and is about 15 miles northeast of Cheyenne in Laramie County, Wyoming. It is a naturally-fractured reservoir, producing oil from the Late Cretaceous Niobrara Formation (Plate I).

## Stratigraphy

The Niobrara Formation in the Denver Basin was deposited in the Late Cretaceous period during a major eustatic sea level rise (Smagala, 1979). Niobrara chalk is a pelagic limestone deposited slowly in an open marine environment where the distribution of these chalks was probably controlled by the terrigenous sediment of western highland or by paleotectonic on lineament-bounded blocks (Pollastro and Scholle, 1984).

Figure 4 shows a generalized stratigraphic column of the Denver Basin (no scale). The Niobrara Formation consists of four limestone (chalk) intervals and three intervening calcareous shales, the thickness of the

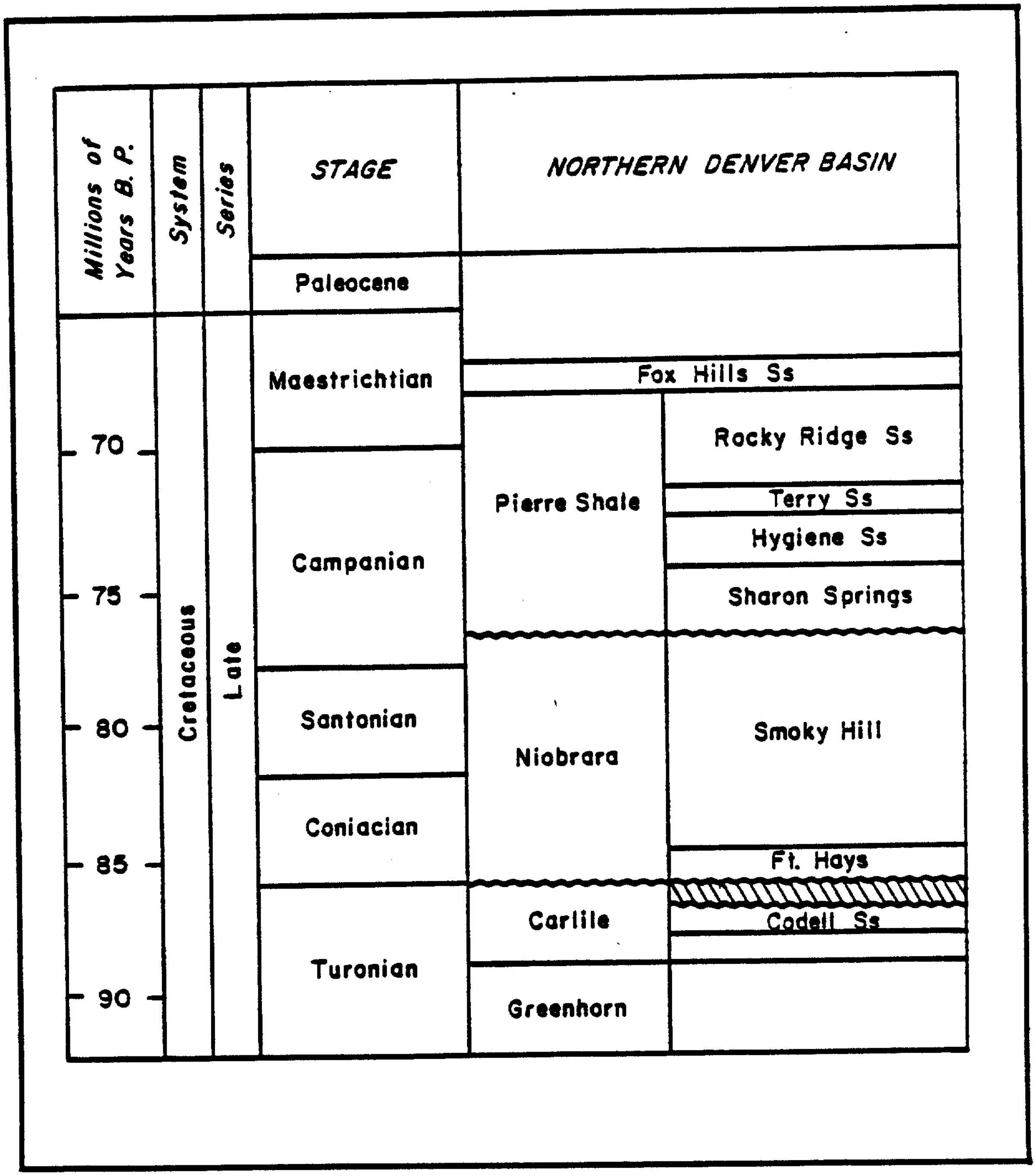


FIGURE 4
GENERALIZED STRATIGRAPHIC
COLUMN OF THE DENVER BASIN
(From Sonnenberg and Weimer, 1981)

Niobrara Formation is about 300 ft in the study area. The lowest chalk is named the Fort Hays, the overlying units are grouped together and named the Smoky Hill Member. The lower boundary of the Niobrara is placed at the base of the Fort Hays or the top of the Codell Sandstone Member of the Carlile Formation. The upper boundary is the contact with noncalcareous black shales of the Pierre Shale and the chalks and calcareous shale of the Niobrara. Both the top and the base of the Niobrara are erosional unconformities. Figure 5 is a partial Late Cretaceous stratigraphic section.

## Structure

The Silo field is on the flank of a paleo-structural high named the Morrill County high (Figure 6). It is located on a small low-relief structure superimposed on gentle regional westerly dip (Figure 7). Figure 8 shows a detailed structure map of the study area controlled by well logs. Structure anomalies reveal the presence of small-scale flexures and small displacement normal faults (Martin, 1987). Weimer (1978, 1980) and others (Silverman, 1984; Merin and Moore, 1986) have related the northeast,

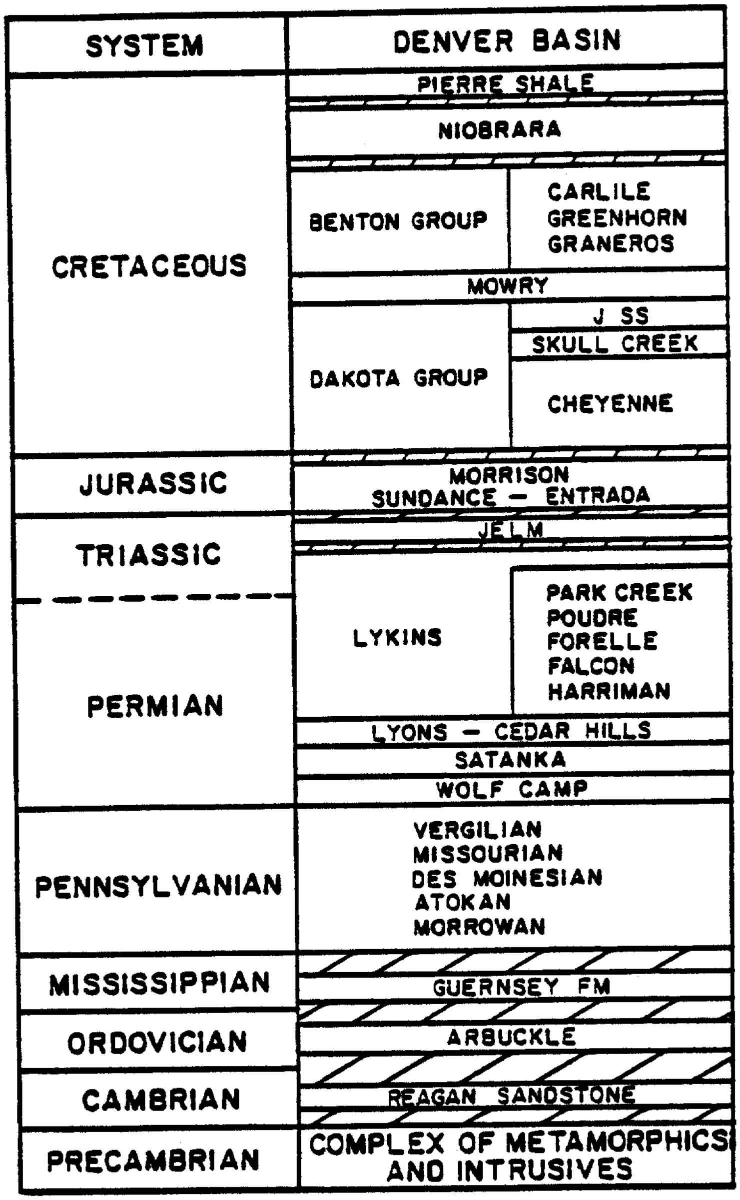


FIGURE 5
PARTIAL STRATIGRAPHIC SECTION OF
THE NORTHERN DENVER BASIN
(From Berman, et al., 1980)

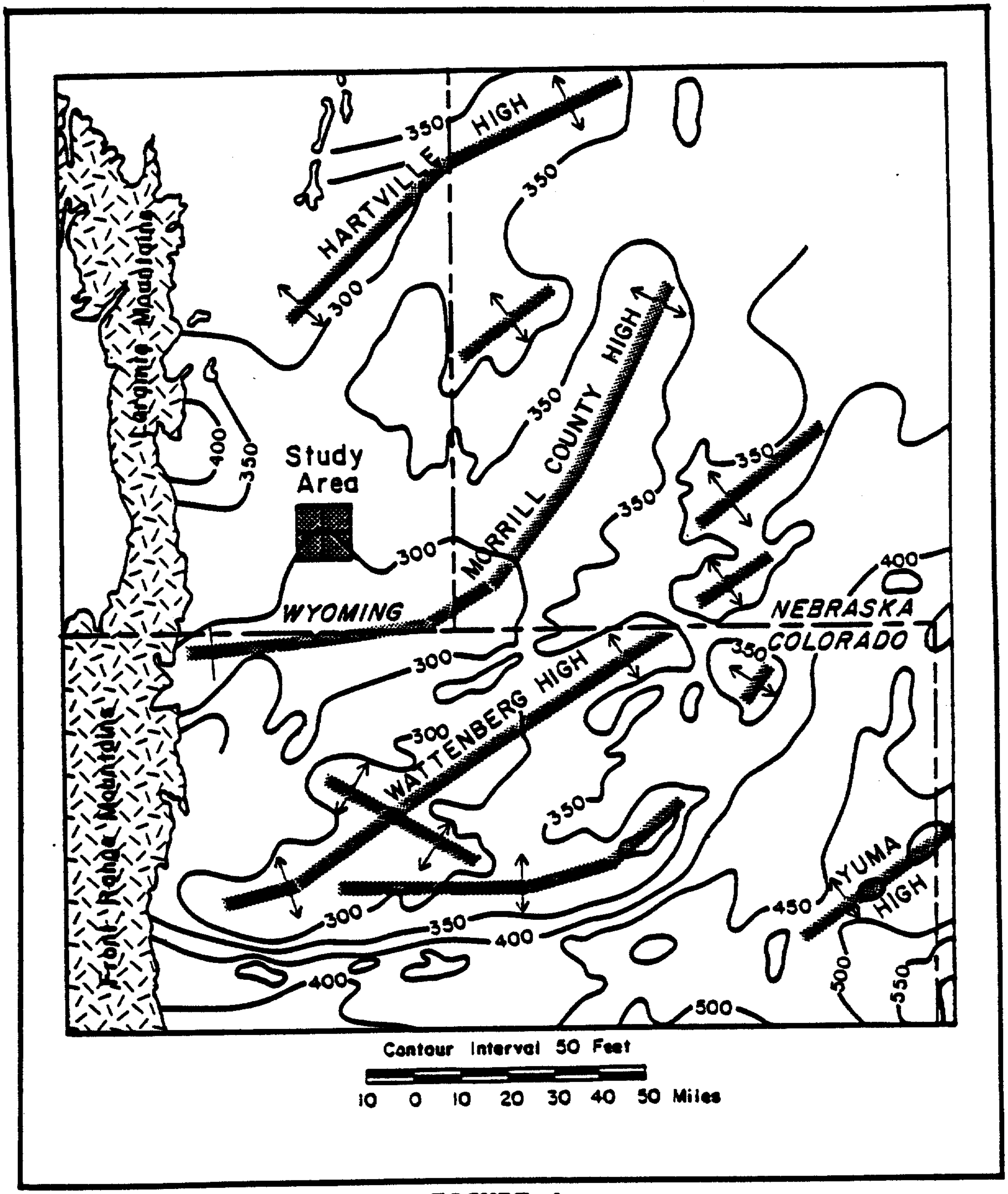


FIGURE 6
REGIONAL NIOBRARA ISOPACH
Showing Structure High and Major
Thinning Trends
(From Sonnenberg and Weimer, 1981)

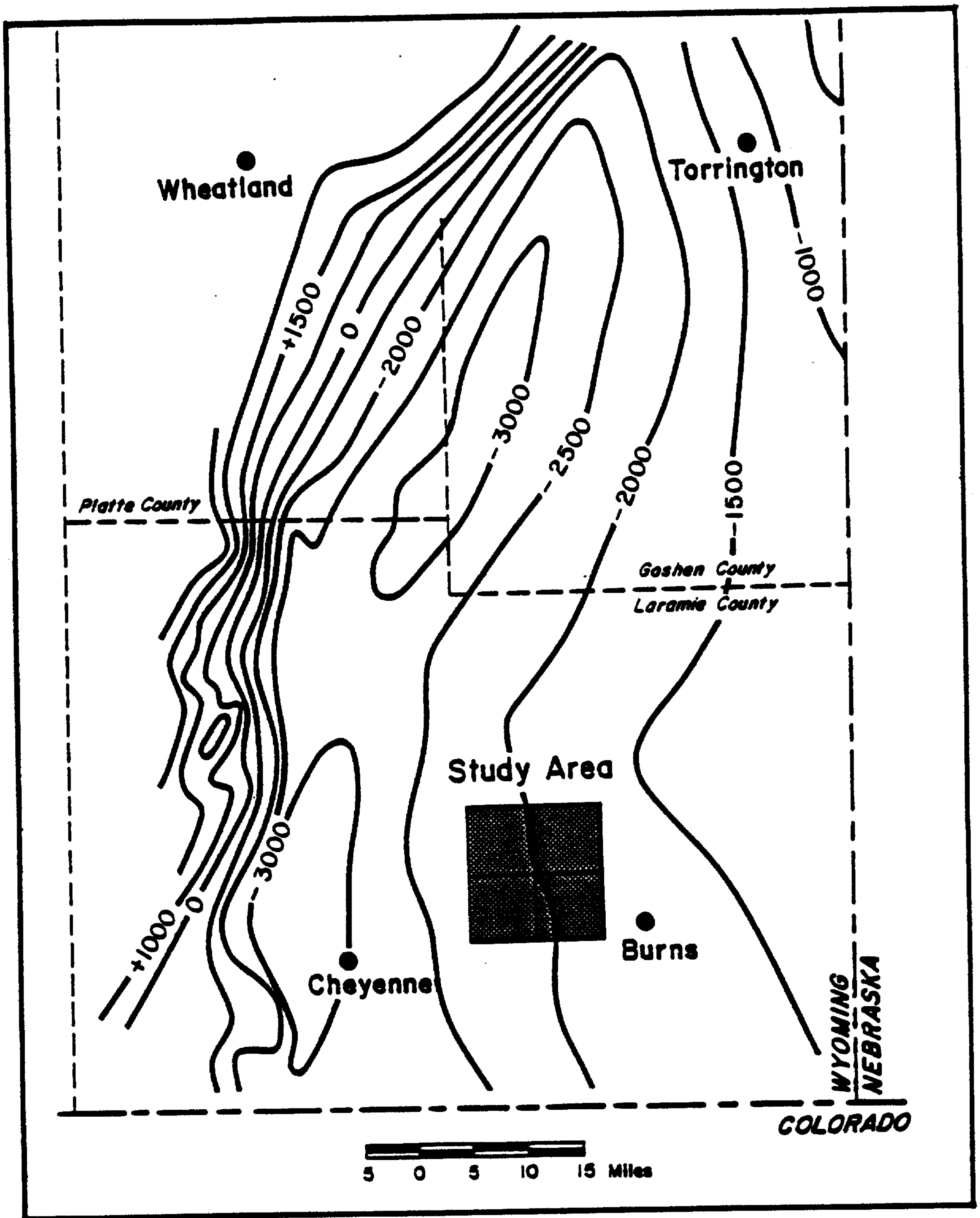


FIGURE 7
REGIONAL NIOBRARA STRUCTURE CONTOUR MAP
(From Merin and Moore, 1986)

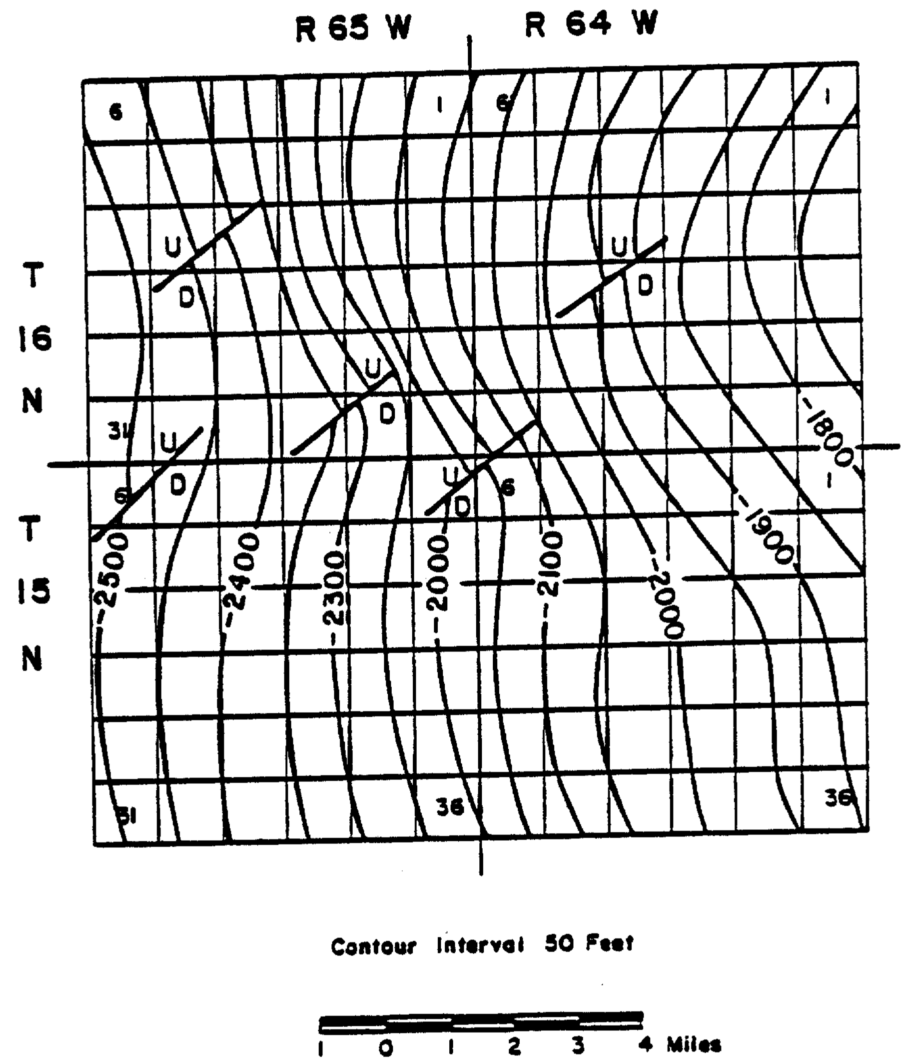


FIGURE 8
STUDY AREA NIOBRARA STRUCTURE CONTOUR MAP
(From Martin, 1987)

northwest and east-west trends of thicker patterns within the Niobrara to recurrent movement on basement fault blocks. Sonnenberg (1981) indicated that the Niobrara was strongly influenced by northeast-trending paleostructure. Merin and Moore (1986) noted that tensional zones in which fracturing exists are coincident with the margins of each of the paleostructures with trends predominantly northeast and northwest. A regional isopach map of the Niobrara Formation shows a major axis of thinning in the northern Denver Basin (Figure 6). Weimer (1978) related this thin to paleotectonic movement on the Transcontinental Arch during Niobrara time. Extensional fracture zones associated with drape folds over basement faults are target areas for future petroleum exploration.

## Hydrocarbon Production and Fracturing

The Niobrara Formation in the deep Denver Basin is rich in organic matter and is considered to be a mature source rock. Fractures parallel to the maximum compressive stress are prime candidates for oil migration and storage in Niobrara Formation. Potential Niobrara reserviors in the deeper part of the Denver Basin occur at a depth in excess of 6,000 to 7,000 ft (Pollastro and

Martinez, 1985). At depths greater than 6,000 ft, reservoir conditions are poor, fractures are required to enable production. Because of the brittleness of the chalk, even minor movement has resulted in significant natural fracturing. Many of the folded structures are further enhanced by numerous normal faults. These fractures cut the brittle Niobrara Formation but generally do not extend into overlying or underlying shales (Pollastro and Scholle, 1985). Oil migration pathways could be both vertically upward or downward from the mature fractured zone of the Niobrara.

Core descriptions from the Amoco 1 State of Wyoming (NENE, Sec. 8, T15N, R64W) and 1 Champlin-300-Amoco-B (SESE, Sec. 5, T15N, R64W) show oil stained, vertical fractures within the Niobrara chalks (Petroleum Information, 1987).

The cumulative oil production in the Silo field is approximately 1 million bbl (Oil and Gas Production Report: Wyoming, Petroleum Information 1987). Figure 9 shows oil production rates in the Silo field. Production rates of all active wells are extremely variable. This variability is directly related to the intensity of natural fracturing in the producing zone. Some geophysical logs designed to detect fractures and

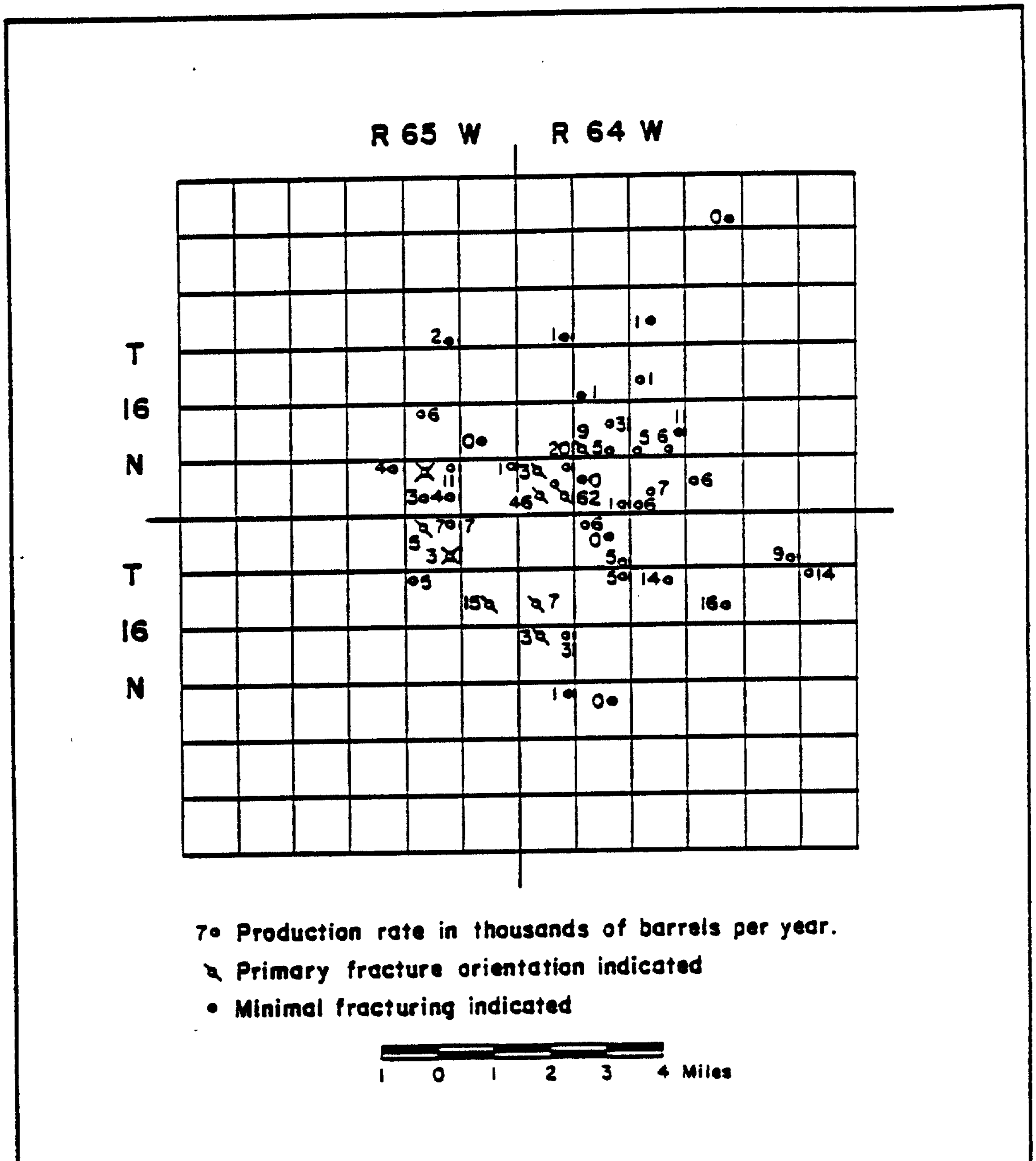


FIGURE 9. PRODUCTION AND FRACTURE ORIENTATION IN SILO FIELD. Oil Production Rates (Through February 1987) and available fracture orientation in the study area (modified from Martin, 1987).

determine their orientation have been run in the Silo field (Petroleum Information, 1987). Examples are: Fracture Identification log, Lithology Cyberlook, Oriented Micro-Resistivity log and Polar Frequency plot (Computer Processed log). Analysis of these log plots for fracture orientation are included in Figure 9. It shows a high frequency of oriented fractures in the northwest-southeast direction associated with relatively good cumulative production (Martin, 1987).

## Well Log Analysis

Figure 10 extracted from the 2 Goertz Leroy C well (Sec. 31, T16N, R64W) represents a typical SP-resistivity log in the Silo field. Four limestone units are easily recognized in the Niobrara Formation because of the higher resistivity of the chalks.

Figure 11 consists of sonic transit time and bulk density logs from the 1 State of Wyoming oil well (NENE, Sec. 8, T15N, R64W) and a dry hole Champlin 300 Amoco C1A (SESE, Sec. 3, T16N, R64W). The thicker B and C chalks account for most of the production within the field. There is little or no differentiation in sonic log or density log response between productive and nonproductive

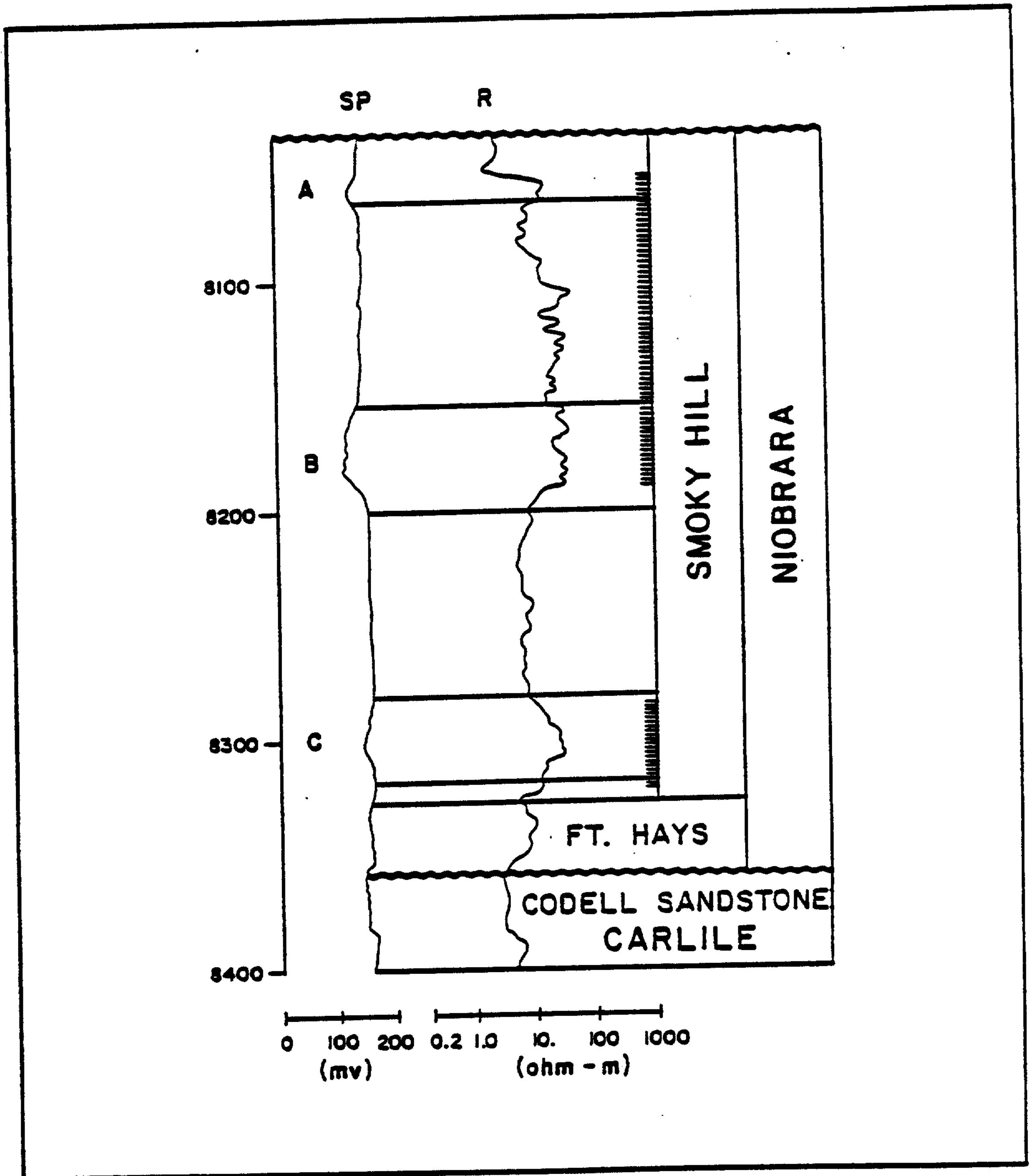


FIGURE 10
TYPICAL NIOBRARA LOG RESPONSES
OF SILO FIELD
Cumulative Production and Perforated
Zones Indicated by Comb Sign.

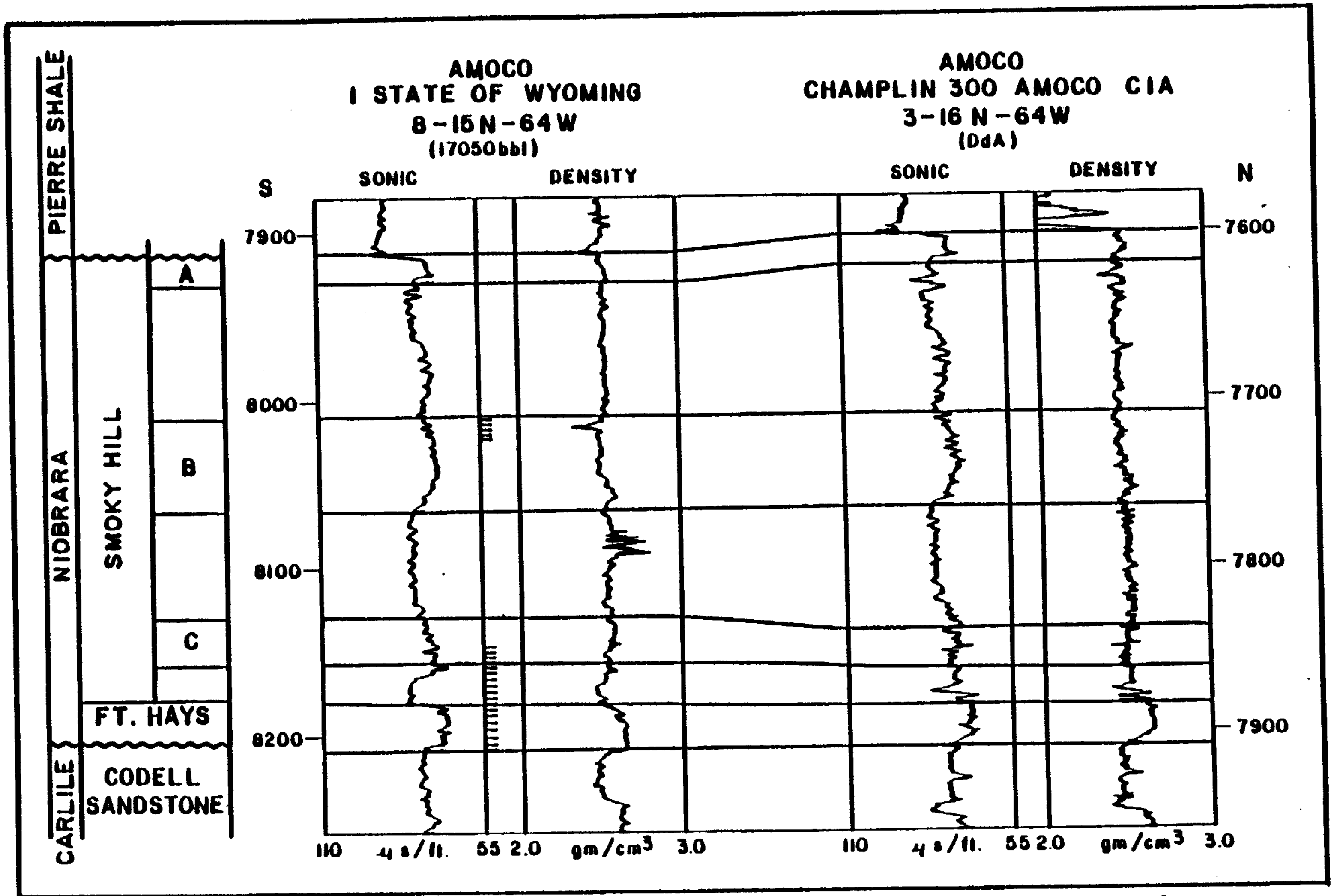


FIGURE 11. SONIC AND DENSITY LOG RESPONSES. For Oil Produced and Non-produced Wells in the Silo Field. Cumulative Production and Perforated Zones Indicated by Comb Sign.

zones in the wells. Therefore, the optimum location to test fracture-controlled production in the Niobrara Formation would be marked by high well-log resistivity and a dense population of intersecting fractures.

## Core Analysis

P-wave velocity, bulk density and S-wave velocity were extracted from an experimental measurement of core from the Golden Buckeye Champlin #9-1 well (NWNE, Sec. 9, T15N, R64W). The measurements were made at PBT Inc. in Golden. Density values were obtained using the Archimedes method. The core sample was weighed dry, wet and jolly (submerged in Sotrol), and porosity was calculated on the basis of the weights.

In the velocity measurements, the transducer arrangement allowed the simultaneous measurements of P-wave and S-wave velocities under the same conditions, the accuracy of the velocity measurement was about 1% for P-wave velocity and 2% for S-wave velocity. Towle (1978) showed that the effective stresses required to make laboratory velocity measurements agree with well log acoustic velocity are on the order of 0.1 or 0.2 psi/ft. The core sample was made in the air, saturated with pore pressure equal to 0 and varying confining pressure of 1,000, 3,000, 4,560, 6,000 psi. The effective stress Pe is given by Pe = Pc - Pp, where Pc is confining pressure, Pp is pore pressure. The commonly used estimate of Pc is 1 psi/ft. Pore pressure is 0.43 psi/ft and the effective pressure is 0.57 psi/ft. The approximate effective pressure is about 4,560 psi for an oil reservoir at 8,000 ft in depth. This relationship holds for well analysis but does not hold for a comparison of laboratory log velocity measurements. Appendix B contains a general description of the core sample and density, porosity and velocity measured values for each case.

# SEISMIC DATA ACQUISTION

Five miles of seismic data for this study were acquired in the Silo field by CGG American Services Inc. Plate I shows the seismic line location in the study area. Appendix A shows the field parameters that were used for the seismic data acquisition. The data were shot as part of a three-component seismic survey (Martin, 1987).

The data were shot with a non-symmetrical split spread with group interval 165 ft and 80 groups, the farthest offset is 13,612.5 ft. The top of the Niobrara Formation is approximately 8,000 ft (O'Rourke, 1986). The largest reflection angle is 41°, which is within the critical angle and wide enough to obtain information from reflections of P- and S (converted waves).

The energy source is Vibroseis #3 Mertz model 18 with source array 330 ft. The sweep frequency is 8-64 herz and the sweep length is 12 seconds. Shot points from 189 to 195 are skipped.

* Trademark of Continental Oil Corp.

# MODELING

The presence of natural fractures in the reservoir is modeled by a transversely isotropic model. The model is isotropic in a plane transverse to a symmetry axis, which can be applied to azimuthally anisotropic media as well as to any material possessing a set of parallel fractures of arbitrary azimuth and dip. The model will be characterized by five elastic parameters and an anisotropy direction which is the normal to the fracture planes (Geoltrain and Bleistein, 1988).

The three independent features of elastic wave propagation in transversely isotropic media are quasi-compressional (qP), transverse and quasi-transverse for each direction of propagation. Those three are polarized in mutually orthogonal directions.

The propagation direction of a plane wave at a given point is the direction of the normal to the wavefront, the direction is also that of the phase velocity. Since the wavefront is nonspherical, that phase angle is different from the group angle (along which energy propagates). From Thomsen (1986) a derivation of the directional dependence of the three phase velocities includes:

$$\rho V_p^2(\theta) = 1/2\,[C_{33} + C_{44} + (C_{11} - C_{33})\sin^2\theta + D(\theta)]$$

$$\rho V_{sv}^2(\theta) = 1/2\,[C_{33} + C_{44} + (C_{11} - C_{33})\sin^2\theta - D(\theta)]$$

$$\rho V_{SH}^2(\theta) = C_{66}\sin^2\theta + C44\cos^2\theta$$

$$\ldots\ldots \quad (5)$$

where $C_{ij}$ are elastic constants of the medium, $\rho$ is density and $\theta$ is the angle between the wavefront normal and the vertical axis, and

$$D(\theta) = \{(C_{33} - C_{44})^2 + 2\,[\,2(C_{13} + C_{44})^2 - (C_{33} - C_{44})\,(C_{11} + C_{33} - 2C_{44})]\sin^2\theta + [(C_{11} + C_{33} - 2C_{44})^2 - 4\,(C_{13} + C_{44})^2]\sin^4\theta\,\}1/2$$

Thomsen (1986) suggested only two elastic moduli (vertical P- and S-wave velocities) plus three measures of anisotropy:

$$\alpha_0 = \sqrt{\frac{C_{33}}{\rho}}$$

$$\beta_0 = \sqrt{\frac{C_{44}}{\rho}}$$

$$\varepsilon = \frac{C_{11} - C_{33}}{2C_{33}}$$

$$\gamma = \frac{C_{66} - C_{44}}{2C_{44}}$$

$$\delta = \frac{1}{2C_{33}^2}\,[2\,(C_{13} + C_{44})^2 - (C_{33} - C_{44})(C_{11} + C_{33} - 2C_{44})] \quad \ldots (6)$$

to simplfly equation 5.

All the phenomena of elastic wavefields in transversely isotropic media can be described in terms of these parameters (notation of Love, 1944 or Thomsen, 1986), density, and propagation orientation relative to the anisotropy axis.

The ray tracing algorithms provide an application of characteristic solutions of the eikonal and transport equations for a set of initial values, given proper initial conditions on amplitude, traveltime, ray Jacobian and slowness direction to trace a ray through a homogeneous medium to the discontinuity surface. At the boundary between media with different elastic properties, the displacements and the stress continuity conditions are applied to determine initial values for tracing the reflected and transmitted waves. Conservation of energy at the interface implies that incident and scattered ray tubes have the same cross sectional areas along the interface and can be used to evaluate the scattering amplitude of the various modes.

The algorithms were implemented to simulate shot profiles over horizontally layered media. The first layer is isotropic for simplicity while the others can be isotropic or transversely isotropic with any fracture azimuth and dip.

Physical values input to the model are from the core sample measurement of Golden Buckeye Champlin #9-1 (NWNE, Sec. 9, T15N, R64W) Appendix B. Cumulative production from the well through March, 1987 is 17,050 bbl (Petroleum Information, 1987). Measured velocity values are obtained from P-wave and S-wave VSP analysis of 2 State of Wyoming Y (Sec. 32, T15N, R64W) (O'Rourke, 1986) Appendix C. Cumulative production from July, 1984 in the 2 State of Wyoming Y well is 163 bbl (Petroleum Information, 1987). A 7-layer model with the upper three layers azimuthal anisotropic and the lower four layers transversely isotropic was derived from the vertical seismic profiles from the same well of Appendix C (Cameron, 1988). A nine-layer model with physical properties as described in Figure 12, travel time for the model was determined using ray tracing of Geoltrain package.

White (1983) conducted a field experiment near Brush, Colorado, for Pierre Shale anisotropy, and concluded that at that location, the Pierre Shale is only exhibited mild P-wave velocity anisotropy. The ratio of the speed of a horizontally traveling compressional wave to the speed of a vertical traveling compressional wave ranges from 1.1 to 1.2. Wright (1987) calculated this anisotropy ratio as 1.06, but the ratio of Austin Chalk is 1.25 (White, 1982).

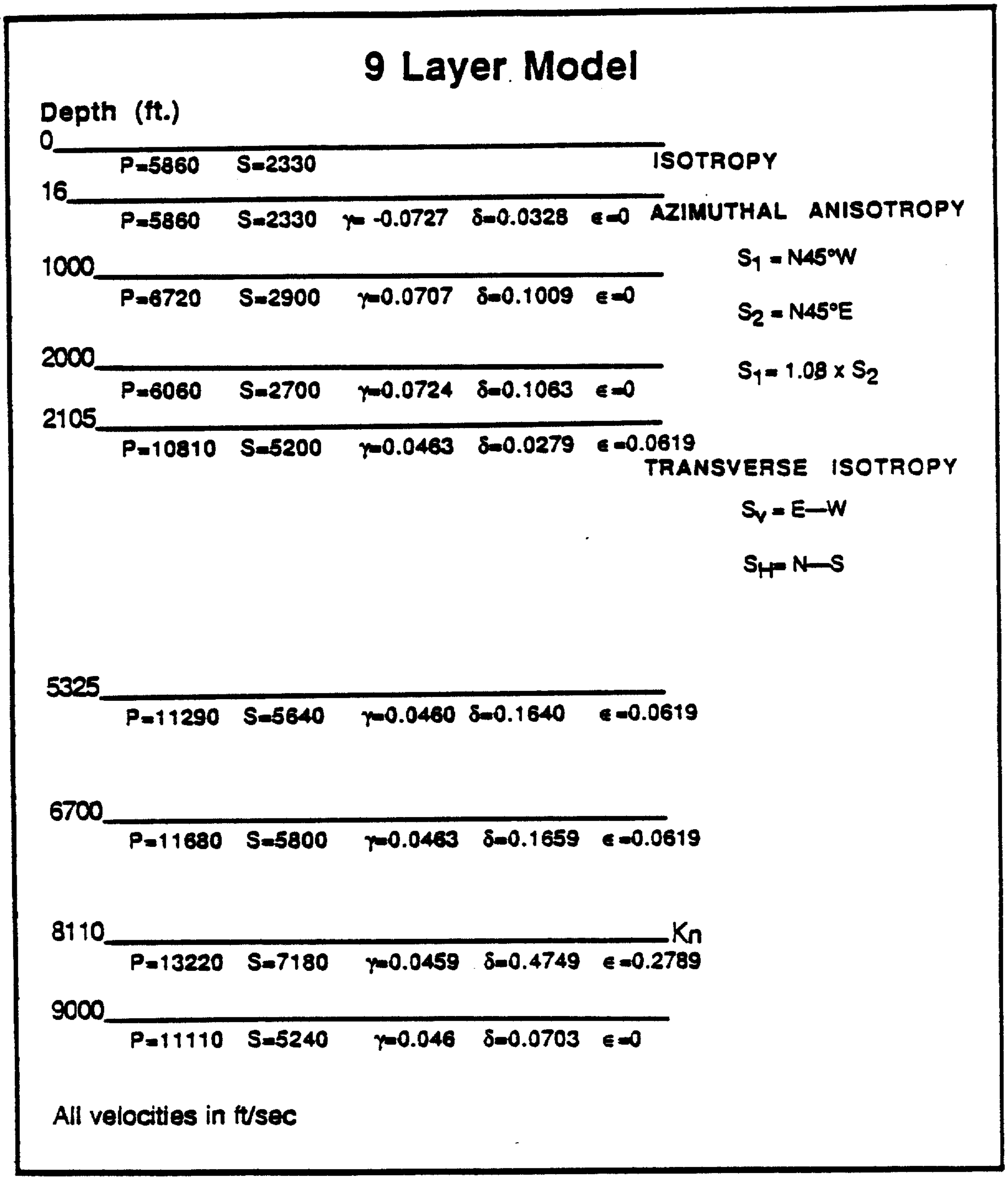


FIGURE 12. GENERALIZED SEISMIC MODEL. The Transversely Isotropic Model in Silo Field, Wyoming (from Cameron, 1988).

In the vertical seismic profile study from the Wyoming Y-2 well, mode converted P-SV provides a shear wave of fixed polarization in the subsurface, regardless of surface anisotropy. The lower Pierre Shale appears fairly isotropic, the Niobrara, Fort Hays and Codell are clearly anisotropic, as evidenced by strong P-SH mode conversions (Iverson, 1988).

A 9,900 ft depth section which included the Pierre Shale and the Niobrara Formation was simulated with a shot record of the farthest offset 10,820 ft (35°). In this nine-layer model, the first layer is assumed isotropic to make the source energy propagation uniform, the second, third and fourth layers are azimuthal anisotropy of S1 = N45 W, S2 = N45 E, Vs1 = 1.08 x Vs2. The fifth to the ninth layer is transversely isotropic with SV = E - W, SH = N - S, the ratio of compressional horizontal to vertical velocities is 1.06 in the Pierre Shale and the ratio is 1.25 in the Niobrara Formation. From the core measurement, the Poisson's ratio of dry to wet sample is from 0.24 to 0.28; water saturation increases Poisson's ratio 17%.

From O'Rourke (1986), the average Poisson ratio of Pierre Shale is 0.34 and in the Cameron layer model (1988), the value also is 0.34. The model was varied by input in the Poisson's ratio 0.34 in Pierre Shale and changing the Poisson's ratio in the Niobrara Formation from 0.20 to 0.30 with increments of 0.01 and keeping the other parameters constant. The rays trace from the surface to the top and the bottom of the Niobrara Formation. Though the polarity is reverse of the conventional, when Poisson's ratio is below 0.24 in the Niobrara Formation, the amplitude decreases with offsets (Figure 13). In Figure 14, when the Poisson's ratio is 0.24, the amplitude is flat in the near offset and increase in the far offset is visible. When Poisson's ratio is 0.25 in the Niobrara Formation, Figure 15 shows an amplitude increase with offset. Amplitude continues to increase with the higher Poisson's ratio in the Niobrara. In the core measurement, the Poisson's ratio of a dry sample is 0.24. This means non-fractured, no fluid saturation. After fluid saturation increases Poisson's ratio, amplitude increases with offset; the greater Poisson's ratio, the greater the amplitude.

Figures 16 and 17 show the seismic characteristic of isotropic and anisotropic Niobrara. If the Niobrara Formation is isotropic, amplitude will decrease with the offset, but in the anisotropic case, as in the transversely isotropic model, the amplitude increases with

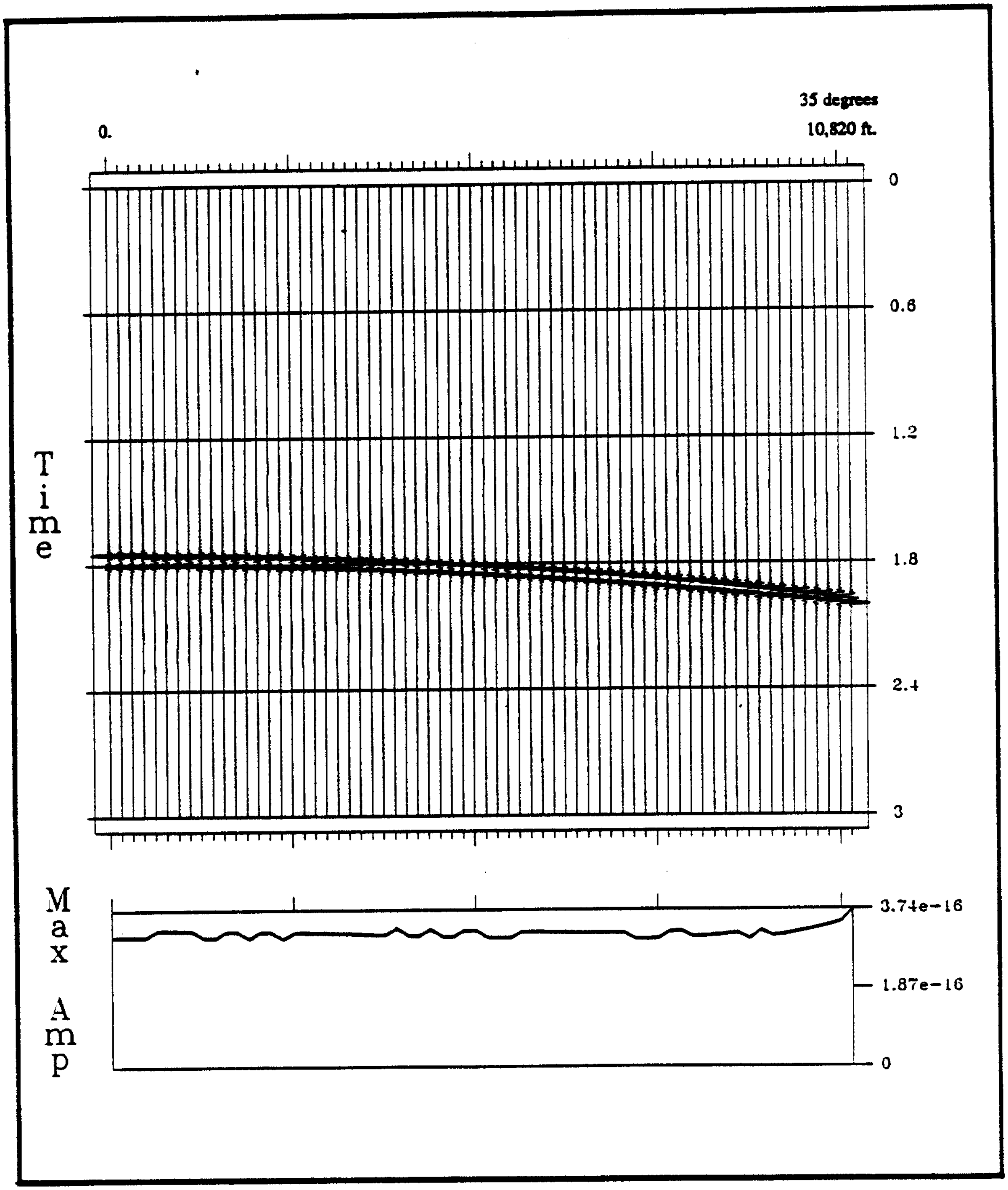


FIGURE 13
SEISMIC CHARACTERISTICS OF TRANSVERSE ISOTROPY
With Kp Poisson's Ratio=0.34,
Kn Poisson's Ratio=0.23

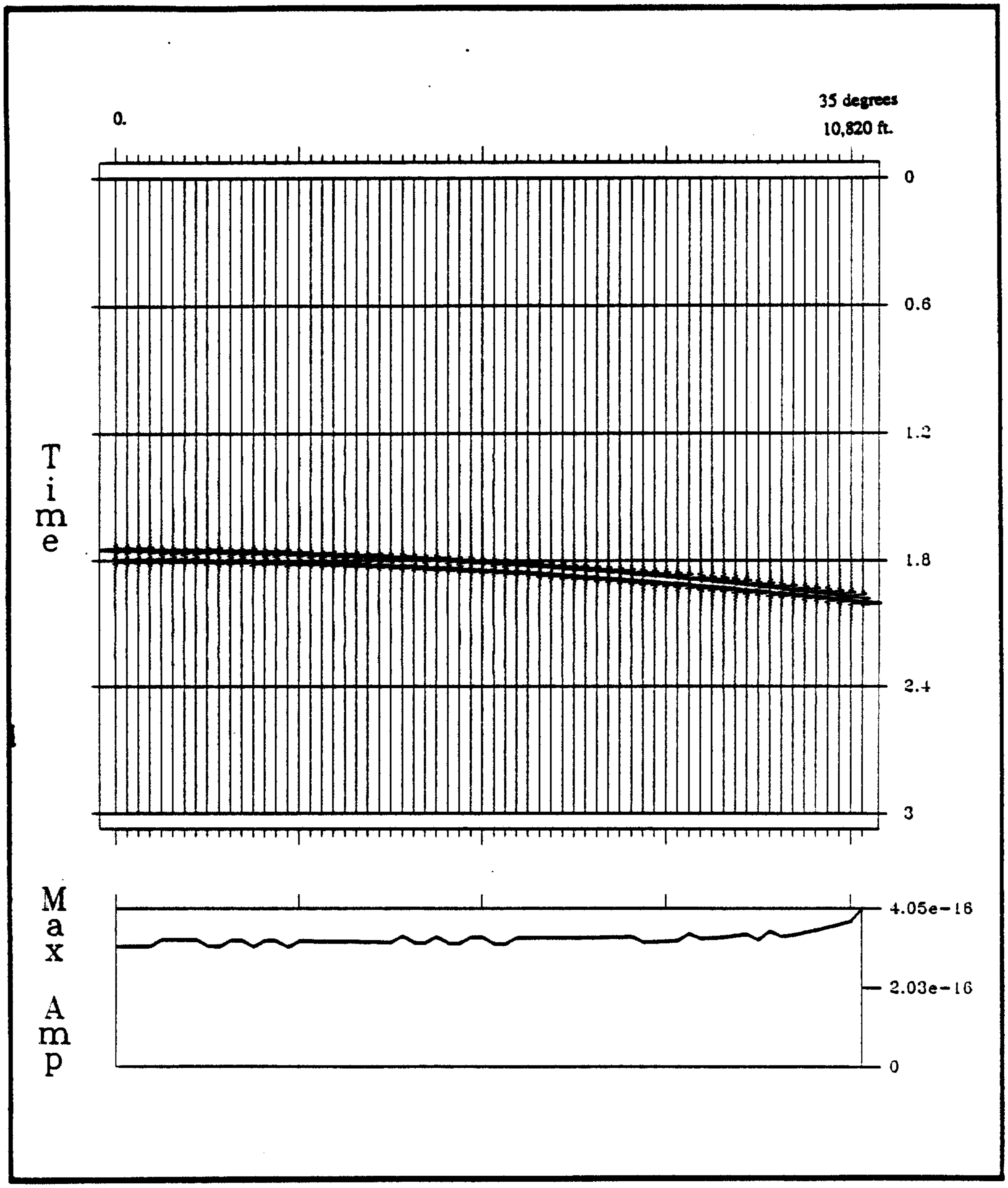


FIGURE 14
SEISMIC CHARACTERISTICS OF TRANSVERSE ISOTROPY
With Kp Poisson's Ratio=0.34,
Kn Poisson's Ratio=0.24

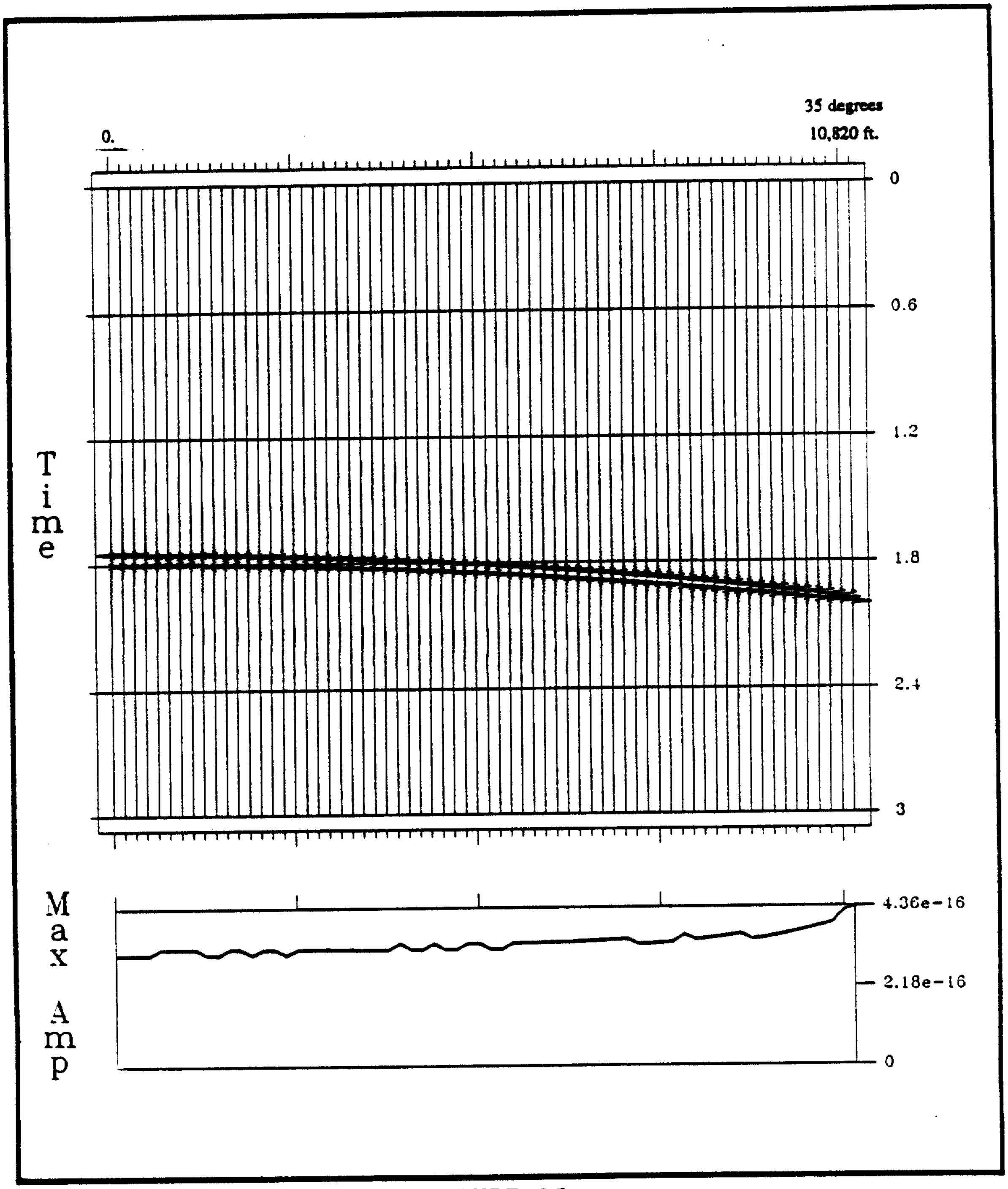


FIGURE 15
SEISMIC CHARACTERISTICS TRANSVERSE ISOTROPY
With Kp Poisson's Ratio=0.34
Kn Poisson's Ratio=0.25

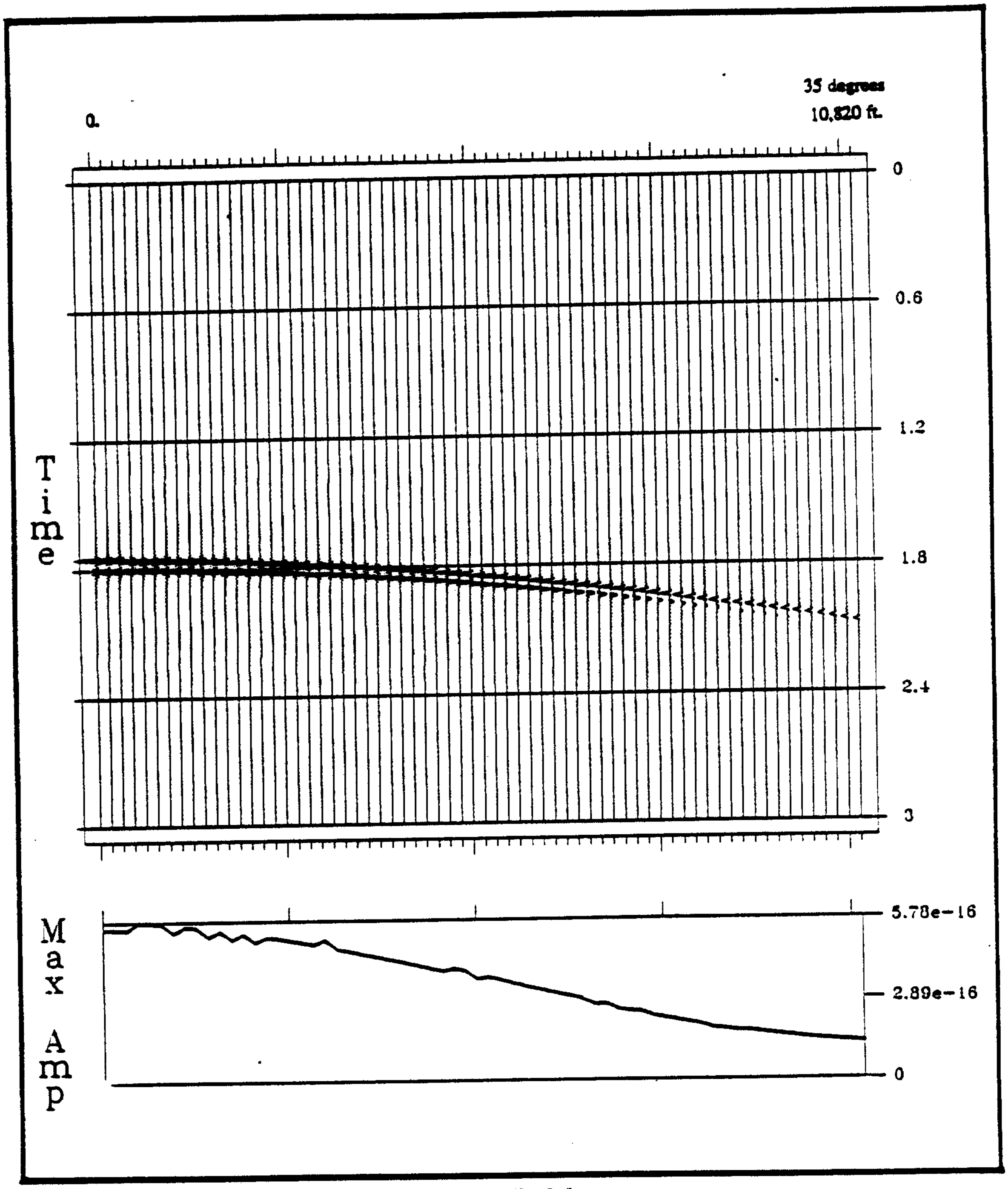


FIGURE 16
SEISMIC CHARACTERISTICS OF ASSUMED ISOTROPIC NIOBRARA

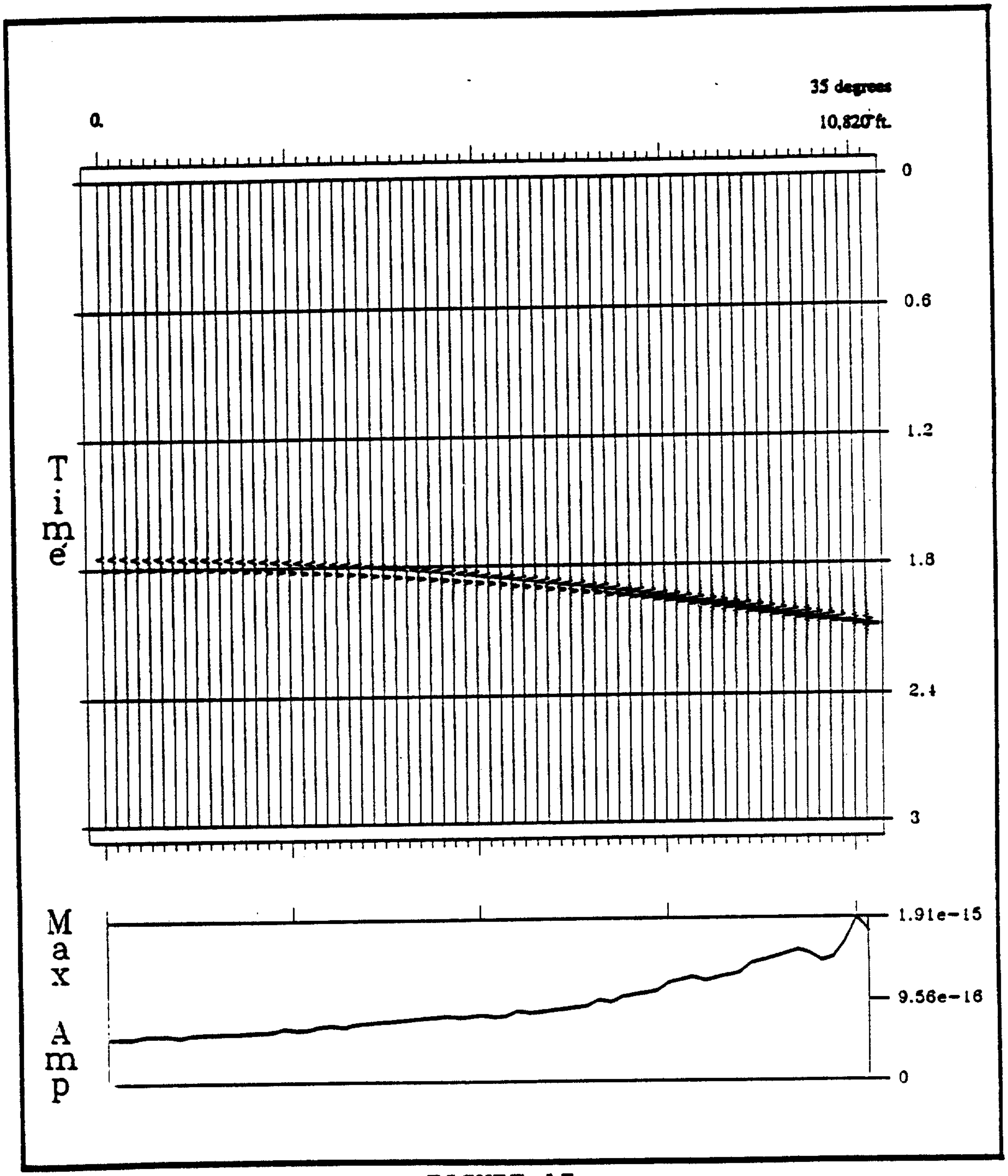


FIGURE 17
SEISMIC CHARACTERISTICS OF TRANSVERSELY ISOTROPIC NIOBRARA

Other Layer Parameters for Model Same as Figure 12.

offset. The scales are different in Figure 16 and Figure 17. In the isotropic case, maximum amplitude concentrates in the normal incidence, and in the anisotropic, increased amplitude is in the far offset. The numerical values of the normal incidence reflection coefficient in both cases can be seen from the fact that the maximum amplitude curves are the same.

Two expressions for the reflection coefficient at the top of the Niobrara are shown in Figure 18 (1). The exact plane wave expression is calculated from Zoeppritz equations in the assumed isotropic Niobrara (2). The exact expression from the model is in the corresponding anisotropic media. Therefore, the reflection coefficient in the anisotropic media is higher than that of isotropic except near the normal incidence, and the critical angle of anisotropic is at 46°, ahead of the isotropic case.

The amplitude increases with offset is a result of the changes in the phase velocity with angle as illustrated in Figure 19, for the QP- and QSV-wave phase velocity of Niobrara. The vertically traveling P-wave has a velocity of 13,218 ft/sec. This velocity increases smoothly to 16,498 ft/sec in the horizontal direction. The effect on the SV phase velocity is even more pronounced, decreasing

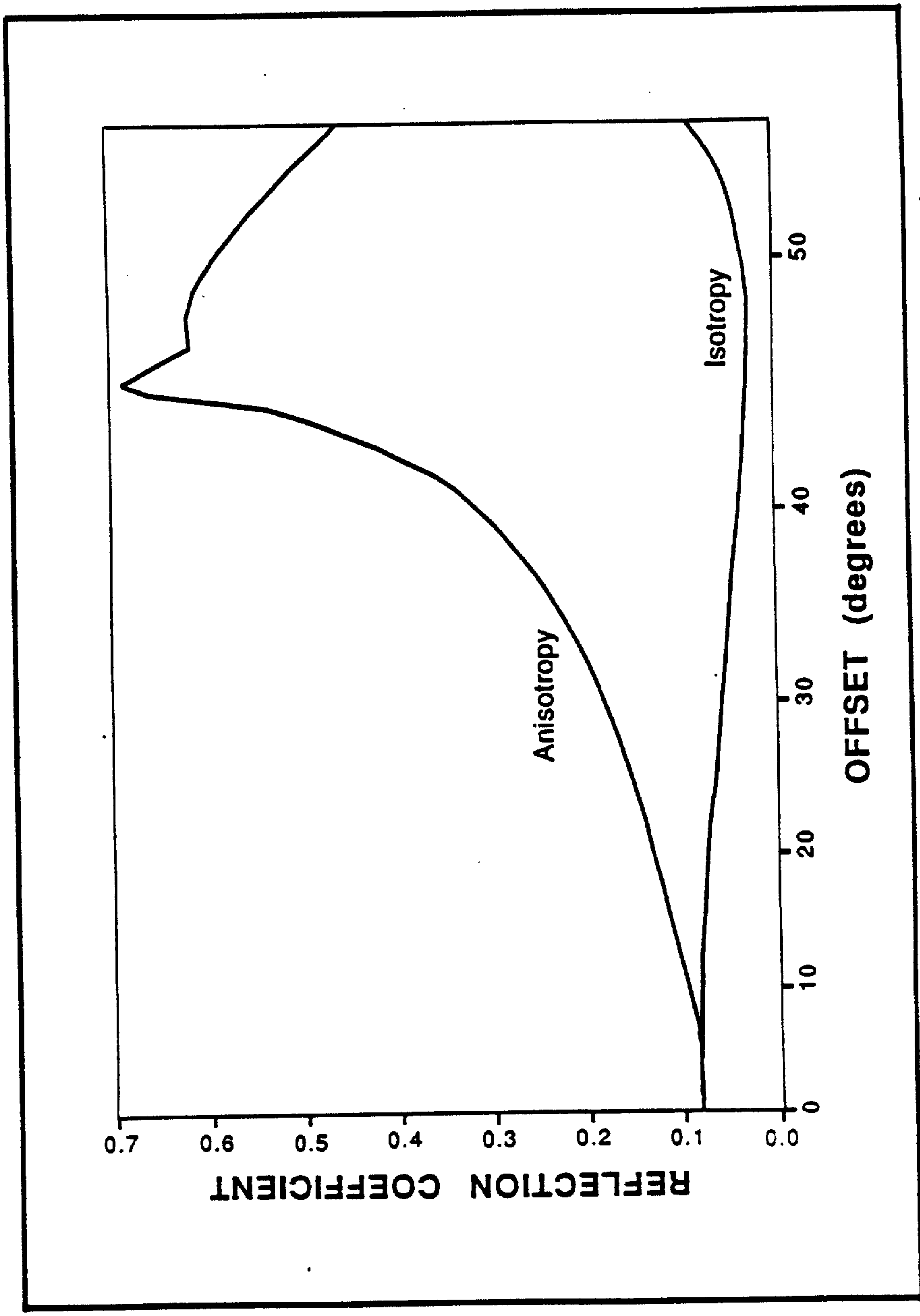


FIGURE 18. REFLECTION COEFFICIENT. With Offset for Isotropic and Transversely Isotropic Niobrara. The Critical Angle of Transversely Isotropic Niobrara is 46°.

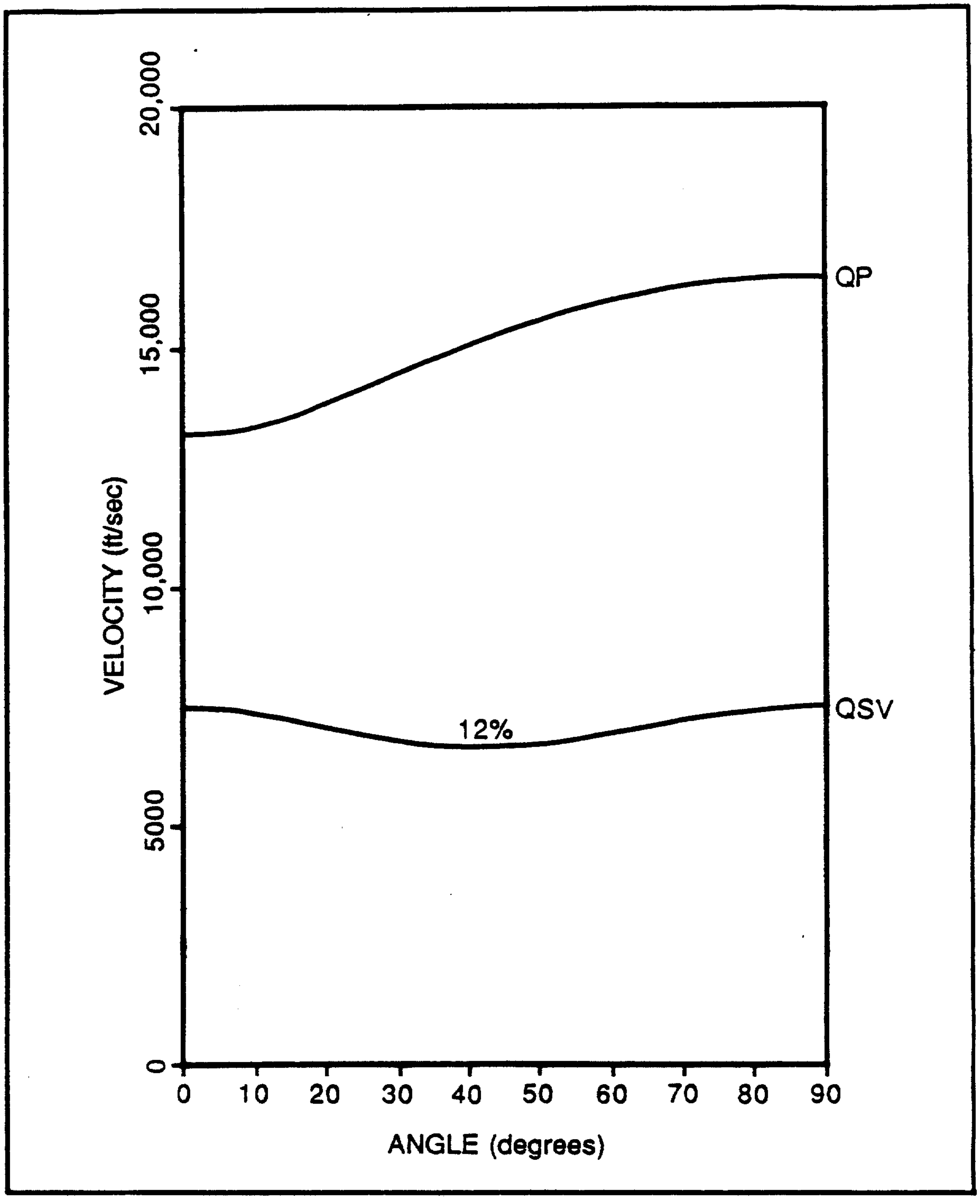


FIGURE 19
QP- AND QSV-WAVE PHASE
VELOCITIES OF NIOBRARA

12% from 0° to 41° from the vertical. This behavior controls the position of the critical angle. Those QP and QSV-wave phase velocities variations cause significant changes in amplitude with offset. Figures 20, 21, and 22 are the amplitude with offset displays for phase at 0°, 45°, and 90°, respectively. They all show amplitude increasing with offset dominant in reflection angle 30° to 35°.

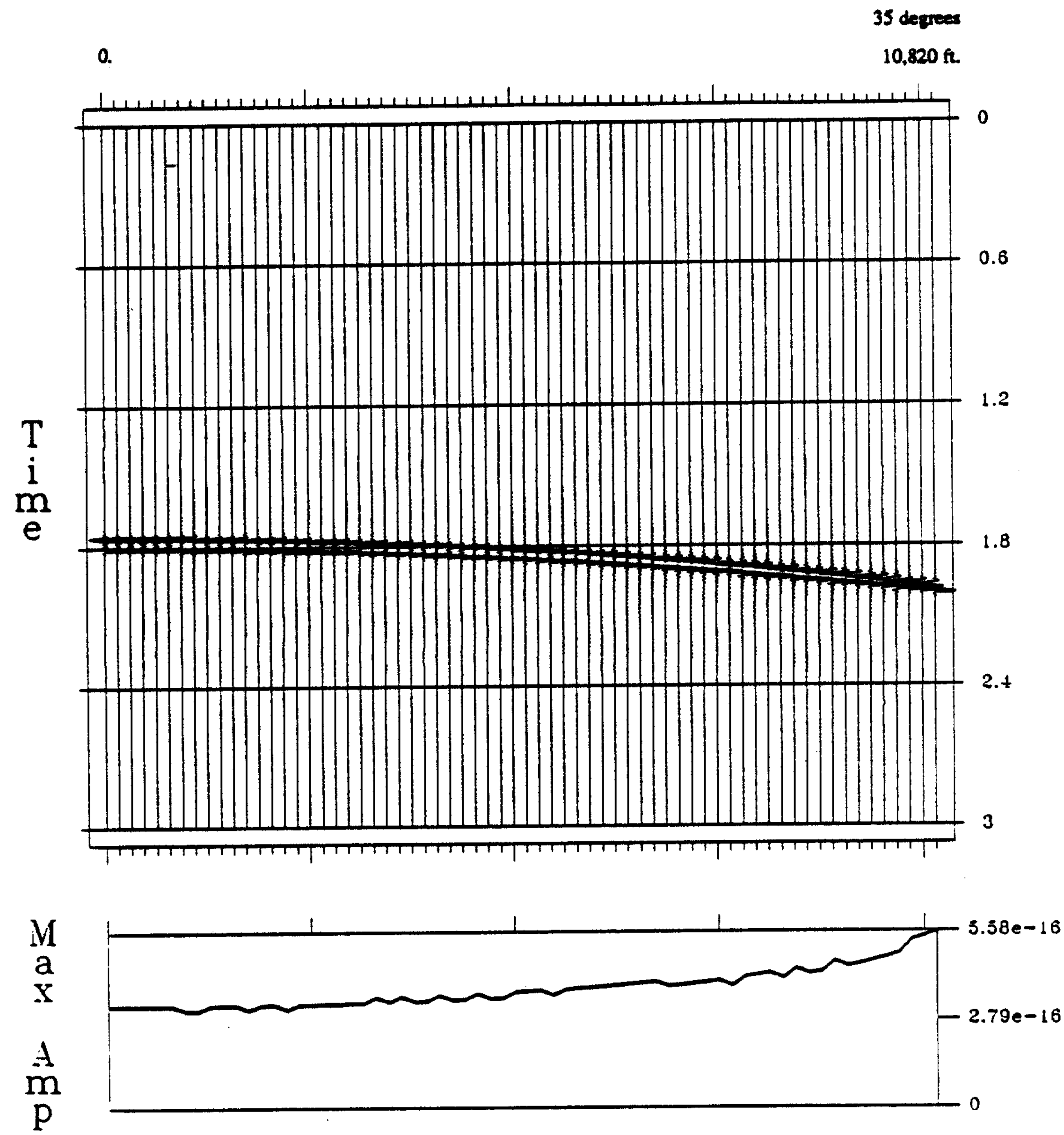


FIGURE 20
AMPLITUDE WITH OFFSET DISPLAY FOR
PHASE VELOCITY AT 0 DEGREE

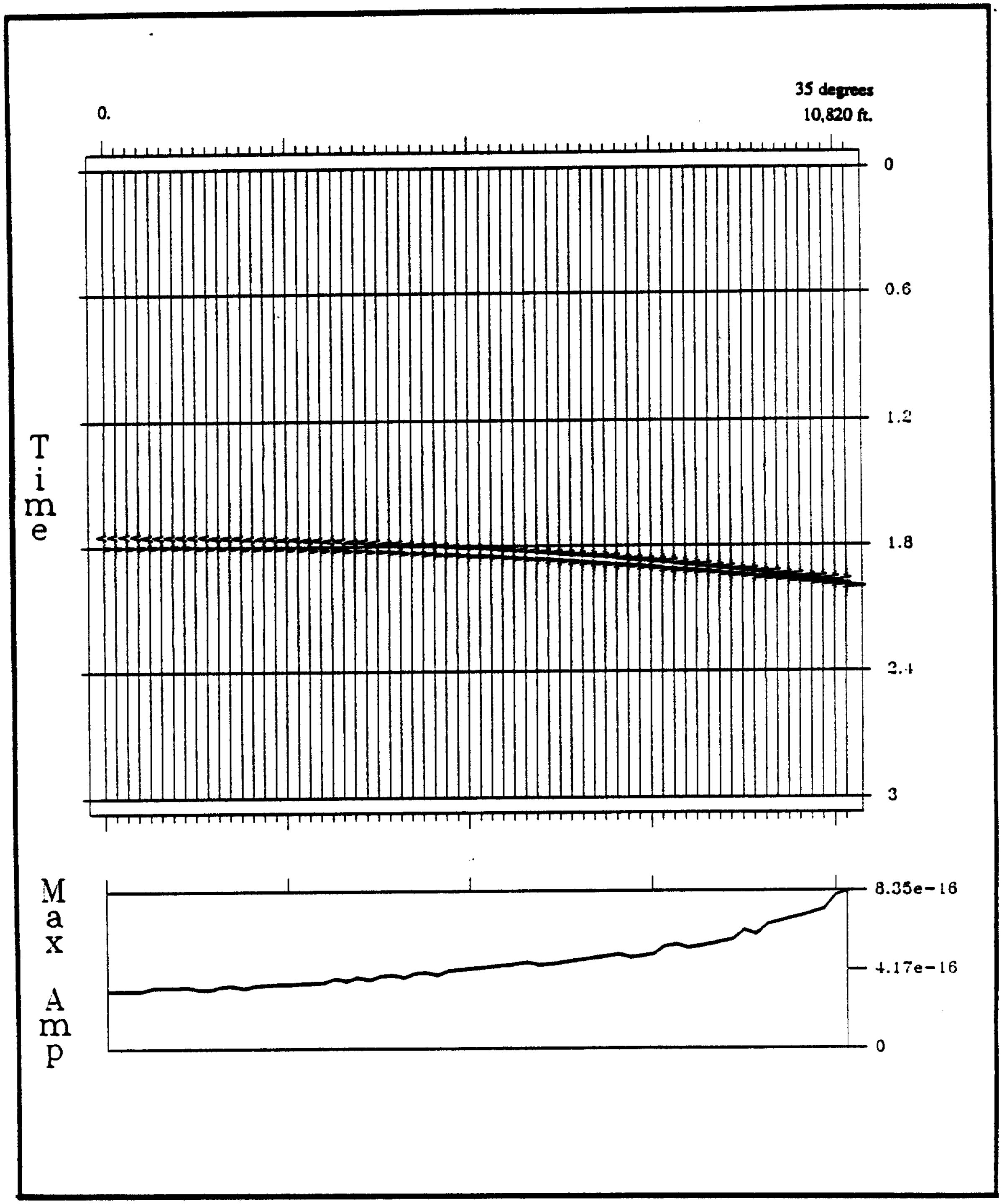


FIGURE 21
AMPLITUDE WITH OFFSET DISPLAY FOR
PHASE VELOCITY AT 45 DEGREES

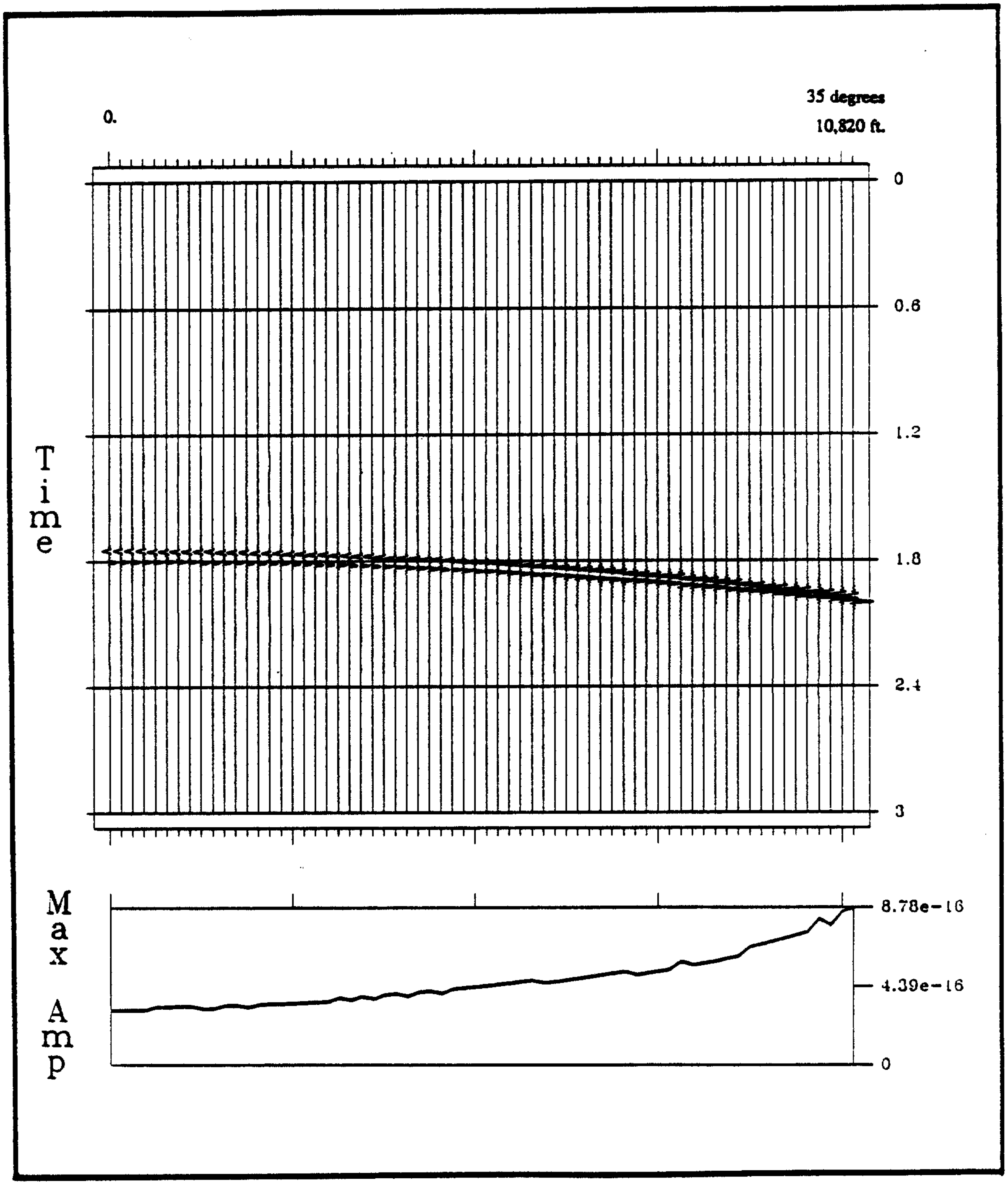


FIGURE 22
AMPLITUDE WITH OFFSET DISPLAY FOR
PHASE VELOCITY AT 90 DEGREES

# SEISMIC DATA PROCESSING

P-wave seismic data processing was done at CGG Data Processing Services in Denver, Colorado, using the GeoMax II* software package. The sequence of data processing and P-wave preserved amplitude stack section are shown in Plate II. This sequence, representing a standard flow for processing seismic data, is emphasized in detailed velocity analysis and preserved amplitude for amplitude with offset analysis.

The main purpose of relative amplitude processing is to restore amplitude losses due to spherical divergence, transmission absorption, etc., without applying AGC scaling in the processing (Newman, 1973).

Statics corrections were estimated from refraction first arrivals and calculated by Gardner's method. Normal moveout was calculated using a linear interpolation routine to obtain the velocity for all points in time. Surface consistent residual static corrections were also derived and applied. Deconvolution of each shot record

*Trademark of CGG.

was conducted by applying the Wiener-Levinson algorithm with a window (200-2,500 ms), 120 ms length operator and 0.1% white noise over the 8/12 - 60/70 Hz bandpass filter.

Single-fold and eight-fold summed gathers of Location A (see Plate II) are shown in Figure 23. On the gathers amplitude increase in the far offset. Though the amplitude of each event in the CDP stack represents an average overall offsets, partial trace sums improves the signal-to-noise ratio for the offset amplitude study.

A strong amplitude increases with increasing offset in fractured zones is apparent in three mixed, one summed gather. Those stacks were generated by using three neighboring CDPS, all common distance within these CDP were stacked together resulting in one trace for each offset distance. This phenomena is better demonstrated when amplitude in a 50 ms window to cover the whole Niobrara formation is numerically plotted against offset distances are shown in Figures 24, 25, and 26. The amplitude decreases with increasing offset in non-fractured zone is shown in Figure 27. The idea comes from Sheriff (1980) that a reflection does not come from a point, but from a zone called the "Fresnel zone" a peak frequency of 40 hz resulted in a Fresnel zone of approximately 600 ft radius at the Niobrara level. This radius might include reflections and diffraction from the

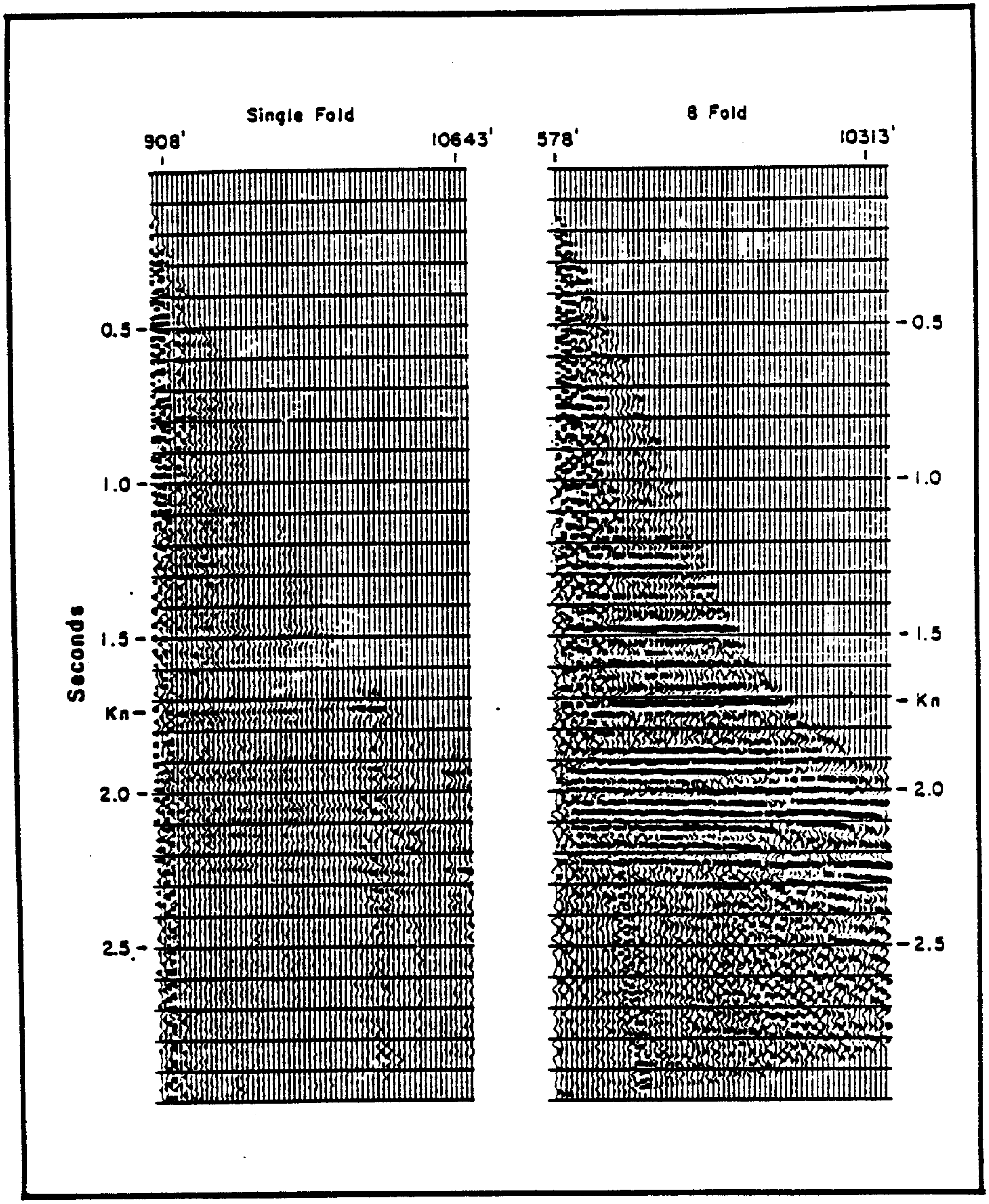


FIGURE 23
COMMON OFFSET STACKS

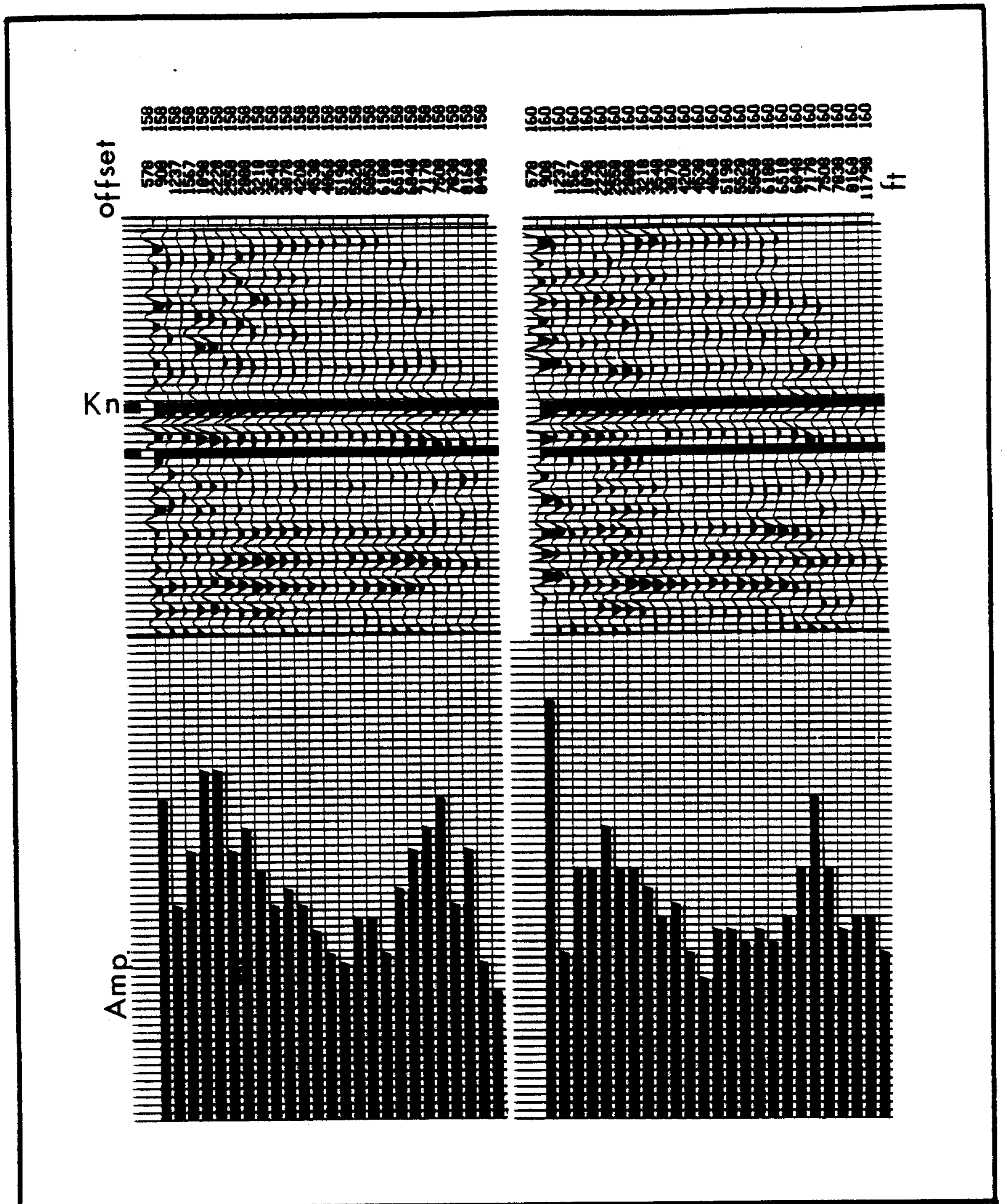


FIGURE 24
NUMERICAL AMPLITUDE DISPLAY.
Against Offset Distance at SP. 158 and 160.

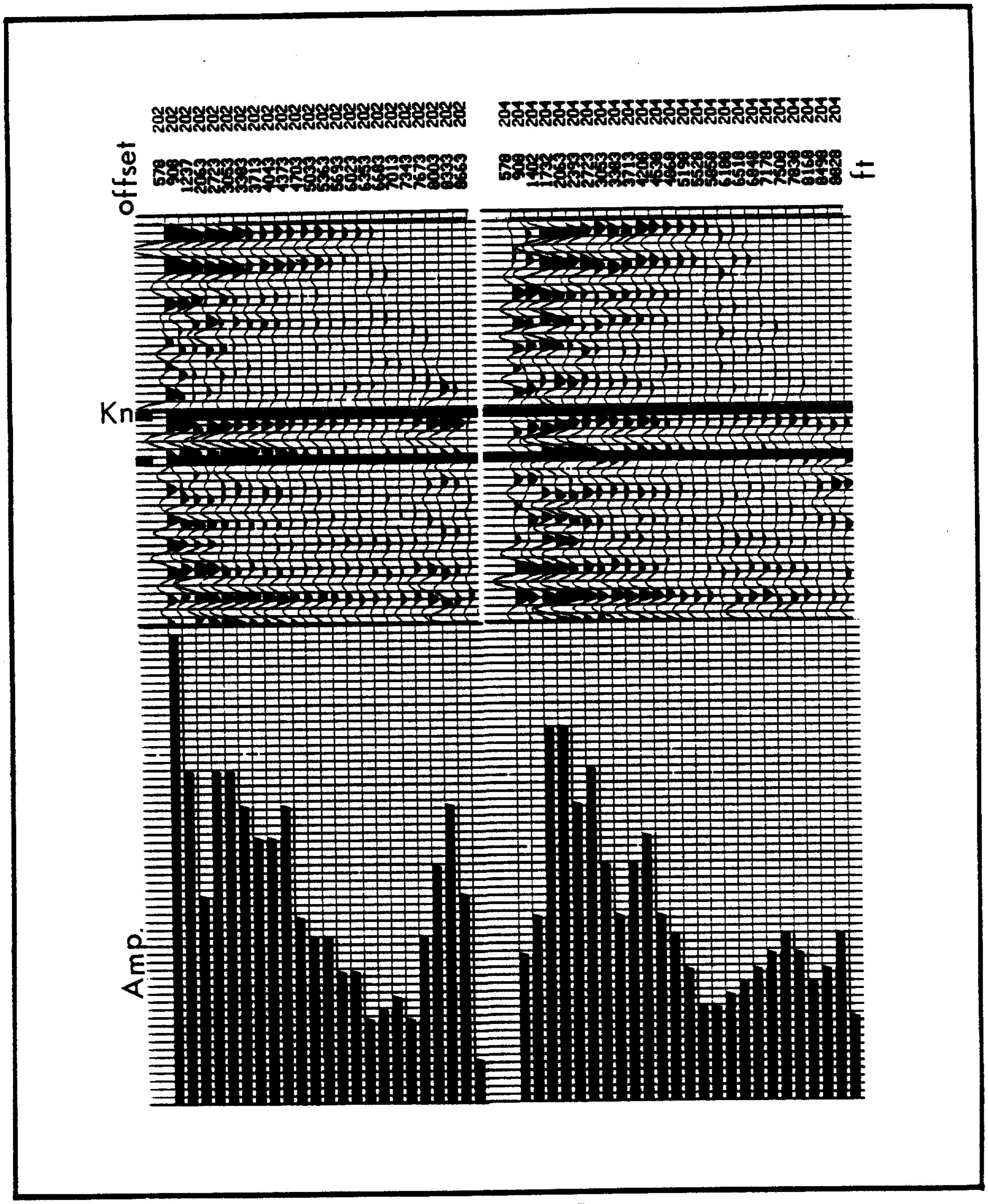

FIGURE 25
NUMERICAL AMPLITUDE DISPLAY.
Against Offset Distance at SP. 202 and 204.

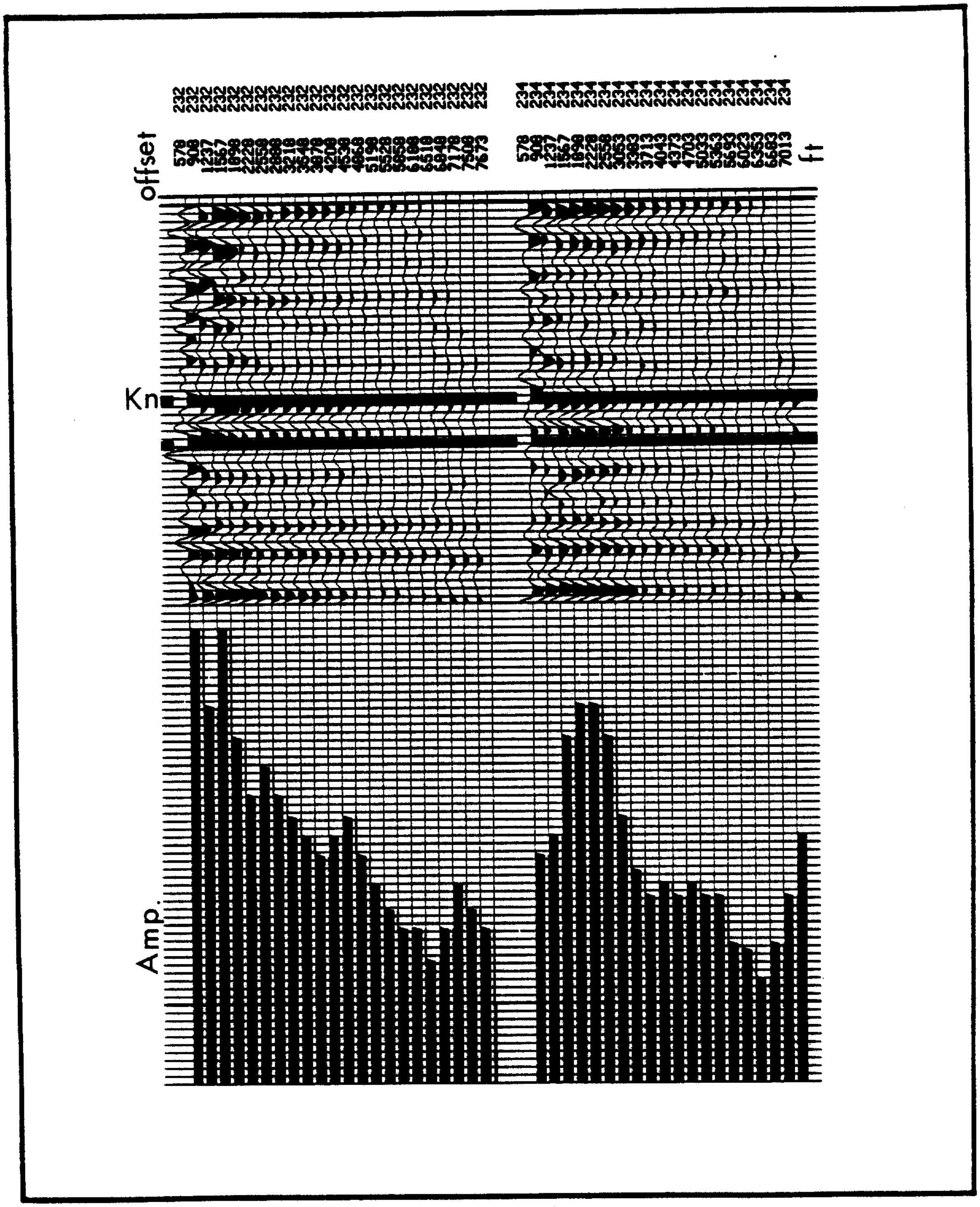


FIGURE 26
NUMERICAL AMPLITUDE DISPLAY.
Against Offset Distance at SP. 232 and 234

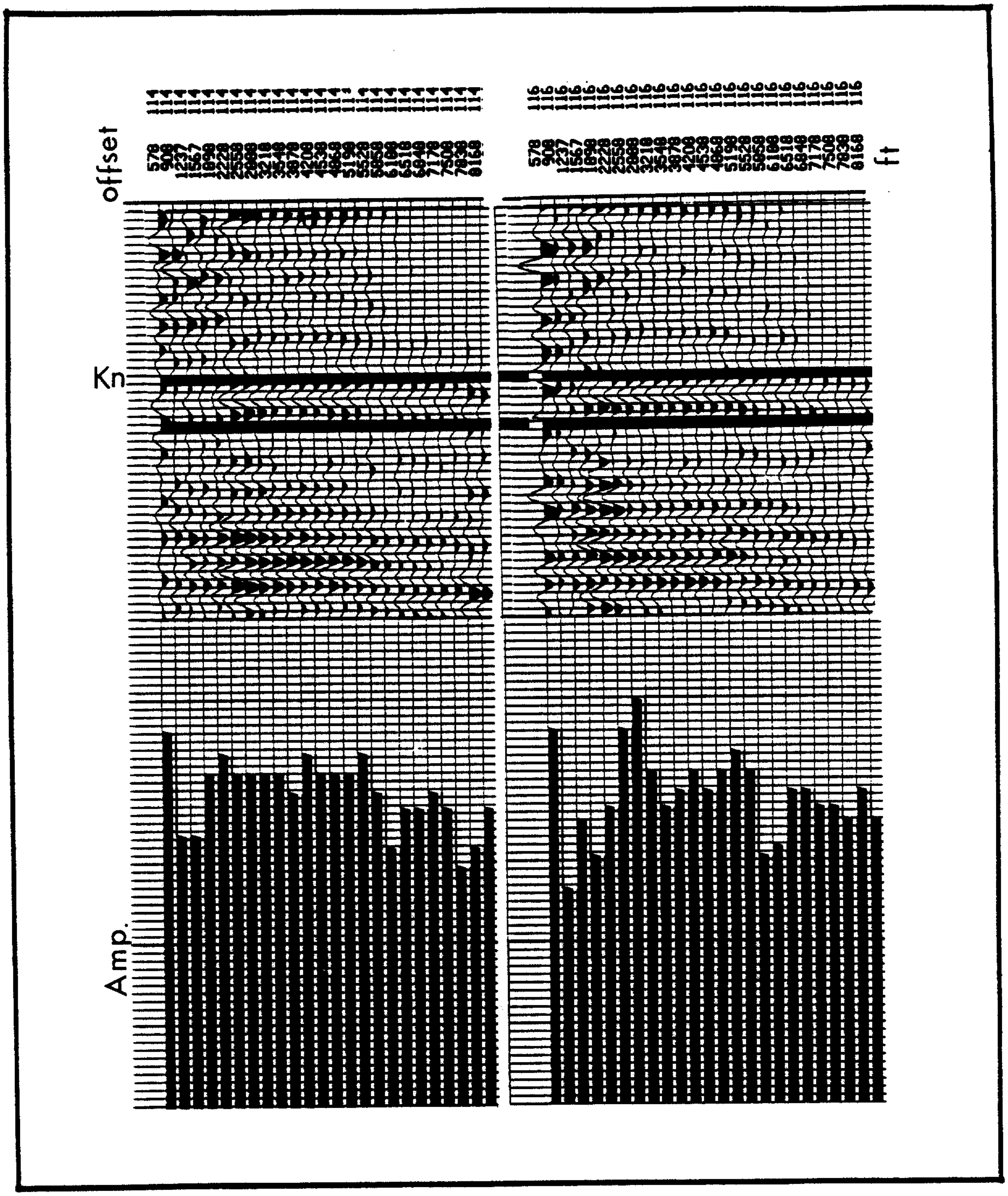


FIGURE 27
NUMERICAL AMPLITUDE DISPLAY.
Against Offset Distance in Non-Fractured
Zone at SP. 114 and 116.

fractures. The amplitude decreases after 7,508 ft in Figure 24 may result from the attenuation of energy.

Figure 28 shows the interval velocity variations within the study window in the seismic line. Sharper contrasts exist within the Niobrara and with adjacent units in fractured zones.

Zero phase characteristics match with a synthetic seismogram produced from sonic and density well logs of 1 State of Wyoming as shown in Figure 29.

After the above processing techniques were applied, the traces were sorted into gathers to form a CDP gather and then stacked. A preserved amplitude stack section in shown in Plate II. The lack of data within shot points 189 to 195 is attributed to the skip and is an unreliable zone for interpretation.

Schneider (1980) suggested the key to understanding the potential for seismic direct detection of hydrocarbon lies in the dependence of velocity and density of a porous material upon the fluid contained in the pore space.

A calculated normal incidence display is a better approximation to the ideal case - a zero offset section. The normal incidence reflection coefficient is directly related to the P-wave velocity and bulk density of the media. The zero offset stack is an ideal case, and the

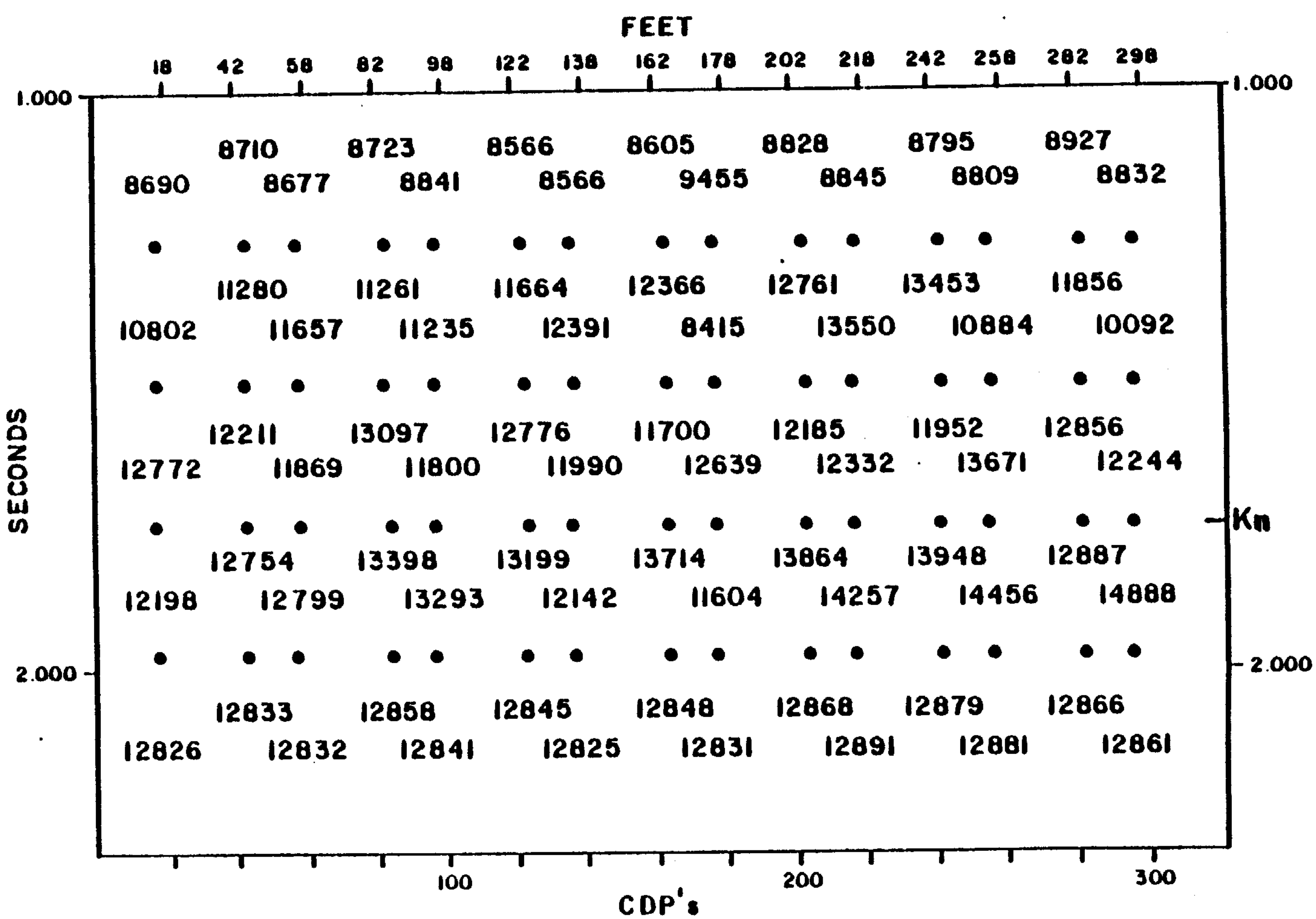


FIGURE 28. P-WAVE INTERVAL VELOCITIES (Feet per Second). From Seismic Data, Posted Between Event Time, Measured From Stacked Section.

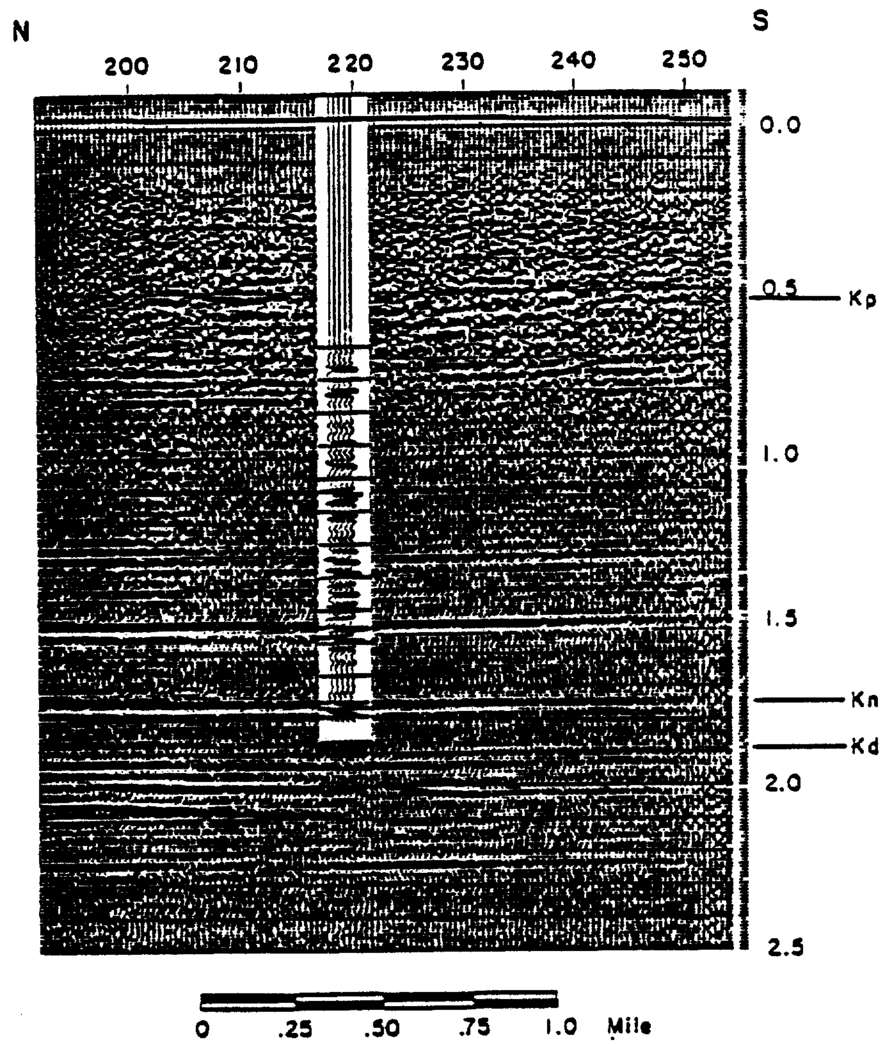


FIGURE 29
PRESERVED P-WAVE SEISMIC SECTION.
Kp=Pierre Shale, Kn=Niobrara, Kd=Dakota.

conventional CDP stack estimates the amplitude of the zero-offset trace by simply averaging overall non-zero offsets.

An alternate method used qualitatively for evaluating amplitude with offset effects is an amplitude difference stack. This stack is generated by taking the difference in amplitude between a far-offset stack and a near-offset stack. In theory, the increase in amplitude with increasing source-to-receiver offset distance should result in an amplitude anomaly on the far-offset stack, not present on the near-offset stack. By taking the difference in amplitude of these stacks, amplitude anomaly with offset will be seen in the fractured areas. In Silo Field, incident angle 40° is approaching the critical angle of reflection P-wave seismic data. The range of the offset for the following discussion is from 10-40°, a wider range can cover more CDP gathers and improve the seismic quality: 10-25°, 10-30°, 10-35°, 10-40° stacks were acquired. The stacks are obtained from CDP gathers and then normalized in the window 1,100-2,300 ms to reduce the effect of noise; then subtraction of the near offset stack from the far offset stack. Amplitude difference sections of 25-30°, 30-35°, and 35-40° are shown in Plates III, IV, and V.

A data file has been established within the Geophysics Department for the volume of data involved in this study. The file contains intermediate processing results and films of the seismic sections used in the study as well as a surface position map of the study area.

# INTERPRETATION

Core studies and fracture identification logs reveal that the Niobrara Formation exhibits mainly vertical fractures in certain areas where the Niobrara is productive. Most producing intervals are located within the 7,700-8,100 ft depth range.

Transversely isotropic modeling of the fractured Niobrara demonstrates that amplitude variations with offset may be an important tool for the identification of fractured and nonfractured regions.

In transversely isotropic media, two very important pieces of information for P-wave reflection prospecting are velocity and reflection amplitude, both of which change in the media. For stresses in the vertical direction, Poisson's ratio $\sigma$ is used to provide the estimate of $C_{13}$ (elastic constant). The relationship between $C_{13}$ and the critical angle is; as $C_{13}$ decreases, the critical angle is smaller. Whereas for the model with the higher $C_{13}$'s, the critical angle will be larger. Poisson's ratio shows the same with $C_{13}$. Therefore, Poisson's ratio can dictate the position of the critical angle. Generally, Pierre Shale has a higher Poisson's ratio ($\sigma$=0.34) than the Niobrara. In the isotropic case, if other physical properties are kept constant, the higher Poisson's ratio causes amplitude to decrease with offset. But, in a transversely isotropic case, Poisson's ratio has the relationship with horizontal compressional and shear wave velocities. The higher the velocity anisotropy, the more the variance of Poisson's ratio thus reversing the trend expected under isotropic conditions. Also, Poisson's ratio has a relationship with fluid saturation. Higher fluid saturation in the Niobrara (Poisson's ratio above 0.24) causes amplitude to increase with offset.

Banik (1987) defined two anisotropy parameters Ep and Es:

$$Ep = (\alpha_h - \alpha_0)/\alpha_0$$

$$Es = (\beta_{45} - \beta_0)/\beta_0$$

where

$\alpha_h$ = P-wave phase velocity in the horizontal direction.

$\alpha_0$ = vertical P-wave phase velocity.

$\beta_{45}$ = SV-wave phase velocity at the angle 45° to the axis of symmetry.

$\beta_0$ = vertical SV-wave phase velocity.

The parameter Ep called "P-wave anisotropy" is approximately equal to the parameter $\varepsilon$ in equation 6.

Es is called SV-wave anisotropy. In Figure 19, phase velocity of Niobrara, Es is negative, Banik emphasized that $\delta$ is an effective anisotropy parameter for P-wave data in the transversely isotropic media, which is roughly the difference between P-wave anisotropy and the QSV-wave anisotropy. In amplitude offset studies, QP-QSV wave mode conversion is an important factor; there is a QP-QSV converted wave, except at the near-normal incidence. In Figure 19, the QSV phase velocity decreased 12% at 41° than in 0°, and QP increases from 0° to 90°. Vp/Vs ratio increased within the critical angle so does Poisson's ratio and makes a significant amplitude increase with offset. Therefore, QSV wave anisotropy greatly influences amplitude-offset effects. Only consideration of P-wave anisotropy may cause erroneous interpretations of reflection amplitude, particularly in the presence of anisotropic media.

In the Niobrara, fractures control oil production. In Plate IV, the 30-35° amplitude difference, shot points 143-161, 164-174, 196-240 have increased amplitudes in the Niobrara. These are interpreted as fractured zones. The amplitude distribution anomaly in shot points 175-190 may result from the skip shot points 189-195; and will not be considered for analysis. Also, from three mixed, one common offset stacks, amplitude increases in the far offset at shot points 158, 160, 202, 204 and 232, 236 are the typical amplitude variations of seismic data in locations A, B, C of Plate II and shown in Figure 24, 25, and 26. Shot points 114, 116 (location D) have decreased amplitudes (Figure 27) which may result from Poisson's ratio smaller than 0.24 or relatively few fractures being present. The information has been transferred to the production map (Figure 9) and is shown in Figure 30 and also shown in Plate I. In Figure 30 from production rate zone A, the production trend is evidently NW-SE. Two wells, 1 Champlin 300-Amoco-B and 1 State of Wyoming are near the south end of the seismic line, their cumulative production are 30,442 bbl and 17,050 bbl respectively and the production zones are Fort Hays (8,174-8,200 ft); and Fort Hays (8,162-8,204 ft) and Codell (8,206-8,234 ft), respectively. To the north, in zone B, Parker 2 cumulative production is 13,844 bbl and the farther north, is zone C, interpreted as having fewer fractures. One well total production is 1,669 bbl (all data through March, 1987, Petroleum Information). Extreme variation of production occurs over short distances, but production data has a good correlation with interpreted fracture locations (Martin, 1987).

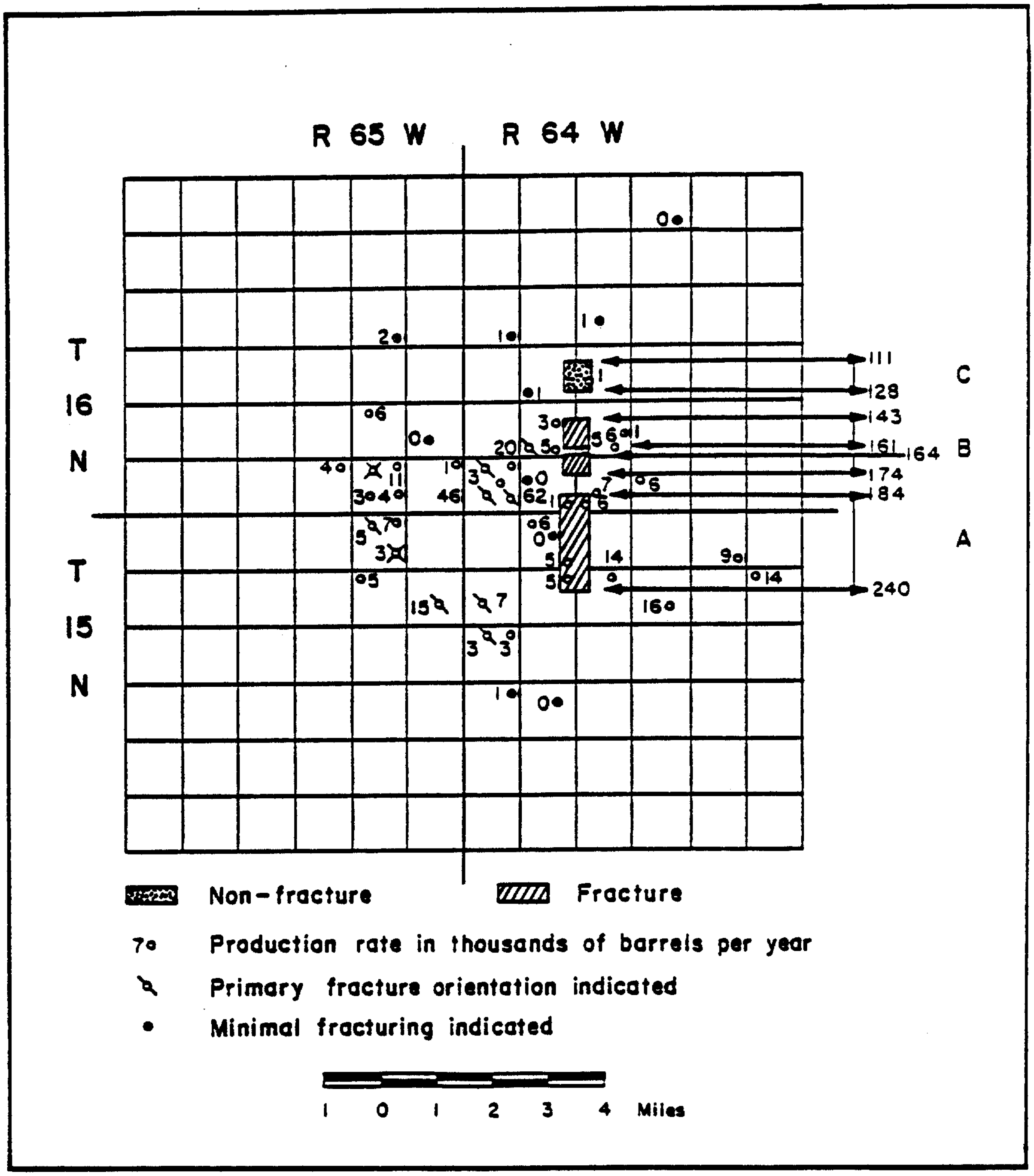


FIGURE 30
PRODUCTION MAP
From Figure 9 With Fracture Zone Locations
Interpreted From Amplitude Display
Data Plate IV.

On the preserved amplitude stack (Plate II) and 30-35° amplitude difference (Plate IV) a stronger reflection at the Niobrara level is considered coincidental with zones of greatest fracture density.

The NW-SE striking fractures may result from recurrent movement on basement fault blocks. Fractures striking NE-SW are probably the result of extension by vertical movement of basement blocks (Sonnenberg and Weimer, 1981). In the fractured Niobrara associated with flexture over basement faults, minor movement and possibly Paleozoic salt dissolution could result in significant fractures. Amplitude and thickness variations in the deep seismic section (2.0 to 2.1 sec on Plate II) suggest the probability of lithologic changes, including possible salt movement. The fractures tend to develop NW-SE and NE-SW (Martin, 1987). Oriented fractures in the NW-SE direction have particularly good cumulative production. P-wave offset amplitude analysis shows the locations of fractures which directly correspond to oil production in the Silo Field.

On Plate III, the 25-30° amplitude display, at 1.2 sec. has the strongest amplitude in the Pierre Shale. White (1982) demonstrated that intrinsic transverse isotropy exists within the Pierre Shale. O'Rourke (1986) identified a zone near the top of the Pierre Shale where VP/Vs ratios were anomalously high. Iverson (1988) depicts that the lower Pierre Shale appears fairly isotropic compared with the upper Pierre Shale. On Plate V, the 35°-40° amplitude display, reflection coefficients are approaching critical angle for most layers. Stronger amplitudes can be seen from Pierre Shale, Niobrara Formation and Dakota group.

In those plates, P-wave data cannot tell us if the fracture's orientation is NW-SE or NE-SW. Thus, through several lines or a 3-D grid seismic exploration may find the exact orientation of fractures.

Results of this study proves that anisotropic properties cause offset amplitude variations and this effect can be used to detect fracture reservoirs. Detailed analysis of P-wave amplitude with offset provides another tool for fractured reservoir evaluation.

# FUTURE WORK

The results of this study suggest the following future work:

Silo Field fracture reservoir is an azimuthal anisotropic case, though the data was simulated with a transversely isotropic model. Amplitude variation in presence of azimuthal anisotropy should be more completely studied.

In this study, Poisson's ratio was kept as a constant, but naturally, it may change within an area. Predicting Poisson's ratio and making iterative Poisson's ratio distribution plots would result in more complete interpretations.

Ostrander (1984) pointed out that only a small percentage of gas in the pore space can alter the offset amplitude relationship. Studies into the influence of fluid saturant in a fracture system on offset amplitude needs to be conducted.

# CONCLUSIONS

The following conclusions are drawn:

1. Results from transversely isotropic modeling indicates that P-wave amplitude may increase with offset in fractured Niobrara zones, and decrease in the non-fractured zones in the Silo Field area, Denver basin, Wyoming.

2. P-wave offset amplitude analysis may provide information on the location and intensity of fracturing in the Silo field.

3. Offset amplitude analysis must consider P-wave and S-wave anisotropy.

4. Offset amplitude depends on the angle of P-wave incidence on the fracture plane.

5. More than one seismic line or a 3-D grid seismic is necessary to tell the orientation of the fractures.

## REFERENCES CITED

Aki, K. and P. G. Richards, 1980, Quantitative seismology: W.H. Freeman and Company, v. 1, p. 123-155.

Banik, D., G. Snyder and W. Barney, 1986, "Examples of a new approach to offset amplitude analysis": paper presented at the 56th annual meeting of SEG.

Banik, N.C., 1987, An effective isotropic parameter in transverse isotropic media, Geophysics, v. 52, p. 1654-1664.

Berman, A.E., D. Pooleschook, Jr., and T.E. Dimelow, 1980, Jurassic and Cretaceous systems of Colorado, in H.C. Kent and K.W. Porter, eds., Colorado Geology: Rocky Mountain Association of Geologists, p. 111-128.

Berryman, J.G., 1979, Long-wave elastic anisotropy in transversely isotropic media: Geophysics, v. 44, p. 896-917.

Bortfeld, R., 1960, "Approximations to the reflection and transmission coefficients of plane longitudinal and transverse waves": Geophys. Prosp., v. IX, p. 485-502.

Cameron, J., 1988 "Shear waves in an anisotropic earth" paper presented at AAPG meeting in Houston, Texas.

Crampin, S., 1977, A review of the effects of anisotropic layering on the propagation of seismic wave, Geophys. J.R. Astro. Soc. v. 49, p. 9-27.

Crampin, S., 1981, A review of wave motion in anisotropic and cracked elastic-media: Wave Motion, v. 3, p. 343-391.

Crampin, S., Stephen, R.A. and McGonigle, R., 1982, The polarization of P-waves in anisotropic media: Geophys. J.R. astr. Soc., v. 68, P. 477-485.

Crampin, S., 1984, "An introduction to wave propagation in anisotropic media": Geophys. J.R. Astro. Soc. v. 76, p. 17-28.

Crampin, S., E.M. Chesnokov and R.A. Hipkin, 1984, "Seismic anisotropy - the state of the art": Geophys. J.R. Astro. Soc., v. 76, p. 1-16.

Crampin, S., 1985, "Evaluation of anisotropy by shear-wave splitting": Geophysics, v. 50, p. 142-152.

Clayton, J.L. and P.J. Swetland, 1980, "Petroleum generation and migration in Denver Basin": AAPG Bulletin, v. 64, p. 1613-1633.

Daley, P.F. and F. Hron, 1977, Reflection and transmission coefficients for transversely isotropic media: Bulletin of the seismological Society of America, v. 67, p. 661-675.

Davis, T.L., P.E. Gretener and R.J. Weimer, 1987, "Seismic exploration: Applications to fractured reservoirs": Continuing Education Courses of SEG.

DeSanto, J.A., 1986, "Mathematics of seismology": Lecture notes, 265 p.

Dix, C.H., 1955, "Seismic velocities from surface measurement": Geophysics, v. 20, p. 68.

Dohr, G. and H. Janle, 1980, "Improvements in the observation of shear waves": Geophys. Prosp., v. 28, p. 208-220.

Domenico, S.N., 1974, "Effect of water saturation on seismic reflectivity of sand reservoirs encased in shale": Geophysics, v. 39, p. 759-769.

Domenico, S.N., 1984, "Rock lithology and porosity determination from shear and compressional wave velocity": Geophysics, v. 49, p. 1188-1195.

Ensley, R.A., 1985, "Evaluation of direct hydrocarbon indicators through comparison of compressional- and shear-wave seismic data: a case study of the Myrnam gas field, Alberta": Geophysics, v. 50, p. 37-48.

Erickson, E.L., D.E. Miller and K.H. Waters, 1968, "Shear wave recording using continuous signal methods part II Later experimentation": Geophysics, v. 33, p. 240-254.

Evans, R., 1984, "Anisotropy: a pervasive feature of fault zones?" Geophys. J.R. astr. Soc. v. 76, p. 157-163.

Gardner, G.H.F., L.W. Gardner and A.R. Gregory, 1974, "Formation velocity and density - the diagnostic basic for stratigraphic traps": Geophysics, v. 39, p. 770-780.

Gassaway, G.S. and H.J. Richgels, 1983, "SAMPLE: Seismic amplitude measurements for primary lithology estimation": SEG National Convention Abstracts, Las Vegas, Nevada, p. 610-613.

Gassaway, G.S., R.A. Brown, and L.E. Bennett, "Pitfalls in seismic amplitude versus offset analysis": Case Histories: paper presented at the 56th Annual Meeting of SEG.

Gassmann, F., 1964, Introduction to seismic travel time methods in anisotropic media: Pure and Appl. Geophys., v. 58, p. 63-112.

Geoltrain, S. and Bleistein, N., 1988 "Aspects of anisotropic wave propagation" paper presented at the 58th annual meeting of SEG.

Graul, M., B. Ostrander and F. Hilterman, 1986, "Seismic lithology": Continuing Education Courses of SEG.

Gregory, A.R., 1976, "Fluid saturation effects on dynamic elastic properties of sedimentary rocks": Geophysics, v. 41, p. 895-921.

Gregory, A.R., 1977, "Aspects of rock physics from laboratory and log data that are important to seismic interpretation, in Seismic stratigraphy - applications to hydrocarbon exploration": Payton, C.E. ed., Am. Assn. Petr. Geol., Memoir 26: p. 15-46.

Hales, A.L. and Roberts, J.L., 1974, "The Zoeppritz amplitude equations; more errors": Bulletin of the Seismological Society of America, v. 64, no. 1, p. 285.

Hamilton, Edwin L., 1979, "Vp/Vs and Poisson's ratios in marine sediments and rocks": J. Acoust. Soc. Am. v. 66, p. 1093-1101.

Hayden, V., 1984, Seismic detection of fractured zones within the Bakken Shale, Antelope field, Williston Basin, North Dakota: M.S. Thesis, Colorado School of Mines, T-2796, 112 p.

King, M.S., 1966, "Wave velocities in rocks as a function of change in overburden pressure and pore fluid saturants": Geophysics, v. 31, no. 1, p. 50-73.

Knott, C.G., 1899, Reflection and refraction of elastic waves with seismological applications: Philos. Mag., v. 48, p. 64-97.

Iverson, W.P., 1988, "Reservoir characterization, Silo Field, Laramie County, Wyoming." Paper presented at Reservoir Characterization Project consortium meeting.

Koefoed, O., 1955, "On the effect of Poisson's ratios of rock strata on the reflection coefficients of plane waves": Geophys. Prosp., v. 3, p. 381-387.

Levin, F.K., 1979, "Seismic velocities in transversely isotropic media": Geophysics, v. 44, no. 5, p. 918-936.

Love, A.E.H., 1944, A treatise on the Mathematical Theory of Elasticity (4th ed.): Dover, New York, NY, 643 p.

Macelwane, J.B. and F.W. Sohon, 1936, Introduction to theoretical seismology: John Wiley & Sons, Inc., p. 147-179.

MacMillan, L., 1980, "Oil and Gas of Colorado: A conceptual view", in H.C. Kent and K.W. Porter, eds., Symposium on the Denver Basin: Rocky Mountain Association of Geologists, v. 2, p. 216-227.

Martin, Marshall A., 1987, Three-component seismic investigation of a fractured reservoir, Silo field, Wyoming: Ph.D Thesis, Colorado School of Mines, T-3339, 99 p.

Martin, Marshall A., and Thomas L. Davis, 1987, Shear-wave birefringence: A new tool for evaluating fractured reservoirs; Geophysics: The leading edge of exploration, October, p. 22-28.

McCormack, M.D., J.A. Dunbar and W.W. Sharp, (1986), "A case study of stratigraphic interpretation using shear and compressional seismic data": Geophysics, v. 49, no. 5, p. 509-520.

Merin, I.S. and W.R. Moore, 1986, "Application of Landsat imagery to oil exploration in Niobrara formation, Denver Basin, Wyoming": AAPG Bulletin, v. 70, p. 351-359.

Muskat, M. and M.W. Meres, 1940, "Reflection and transmission coefficients for plane waves in elastic media": Geophysics, v. 5, p. 115-133.

Nafe, John E., 1956, "Reflection and transmission coefficients at a solid-solid interface of high velocity contrast": Bulletin of the Seismological Society of America, p. 205-219.

Newman, p., 1973, "Divergence effects in a layered earth": Geophysics, v. 38, p. 481-488.

O'Connell, R.J. and B. Budiansky, 1974, "Seismic velocities in dry and saturated cracked solids": Journal of Geophysical research, v. 79, p. 5412-5426.

O'Rourke, T.J., 1986, Shear and Compressional analysis of VSP in Silo field, Denver-Julesburg Basin: M.S. Thesis, Colorado School of Mines, T-3198, 93 p.

Ostrander, W.J., 1984, "Plane-wave reflection coefficients for gas sands at nonnormal angles of incidence": Geophysics, v. 49, p. 1637-1648.

Pickett, G.R., 1963, "Acoustic character logs and their applications in formation evaluation": J. Petr. Tech., v. 15, p. 659-667.

Pollastro, R.M., and C.J. Martinez, 1985, "Mineral, chemical and textural relationships in rhythmic-bedded hydrocarbon productive chalk of the Niobrara formation, Denver Basin, Colorado": The Mountain Geologist, v. 22, p. 55-63.

Pollastro. R.M., and P.A. Scholle, 1984, "Hydrocarbons exploration, development from low permeability chalks, upper Cretaceous Niobrara formation, Rocky Mountain region": Oil and Gas Journal, v. 82, p. 140-145.

Postma, G.W., 1955, Wave propagation in a stratified medium: Geophysics, V. XX, p. 780-806.

Richter, C.F., 1958, Elementary seismology: p. 670-673.

Schneider, W.A., 1980, "The reflection seismic prospecting system": Colorado School of Mines Press.

Sheriff, R.E., 1980, Nomogram for Fresnel-zone calculation: Geophysics, v. 45, p. 968-972.

Shuey, R.T., 1985, "A simplification of the Zoeppritz equations": Geophysics, v. 50, p. 609-614.

Silverman, M.R., 1984, "Petroleum geology and exploration of Scotts Bluff trend, northeastern Denver basin, Nebraska": AAPG Bulletin, v. 68, p. 527-528.

Smagala, T. and M.B. Cooper, 1979, "The Cretaceous Niobrara play": Transmission Conference of the American Gas Association, New Orleans, Louisiana, 42 p.

Smagala, Tom, 1981, "The Cretaceous Niobrara play": Oil and Gas Journal, p. 204-218.

Sonnenberg, S.A., and R. J. Weimer, 1981, Tectonics, sedimentation and petroleum potential, northern Denver basin, Colorado, Wyoming, and Nebraska: Colorado School of Mines Quarterly, v. 76, no. 2 45 p.

Taner, M.T. and F. Koehler, 1969, "Velocity spectra-digital computer derivation and applications of velocity functions": Geophysics, v. 34, p. 859-881.

Tatham, Robert H. and Paul L. Stoffa, 1976, "Vp/Vs-A potential hydrocarbon indicator": Geophysics, v. 47, p. 336-344.

Tatham, Robert H., 1982, "Vp/Vs and lithology": Geophysics, v. 47, p. 336-344.

Towle, G.H., 1978, Stress effects on acoustic velocities of rock: Ph.D Thesis, Colorado School of Mines, T-1702, p. 49-77.

Thomsen, L., 1986, "Weak elastic anisotropy": Geophysics, v. 51, p. 1954-1966.

Waters, K.H., 1978, Reflection seismology: a tool for energy resource exploration: p. 39-40.

Weimer, R.J., 1978, "Influence of transcontinental arch on Cretaceous marine sedimentation: A preliminary report": in J.D. Pruit and P.E. Coffin, eds., Symposium on energy resources of Denver basin: Rocky Mountain Association of Geologists, p. 211-221.

Weimer, R.J., 1980, "Recurrent movement on basement faults, a tectonic style for Colorado and adjacent areas": in H.C. Kent and K.W. Porter, eds., Symposium on the Denver basin: Rocky Mountain Association of Geologists, p. 23-35.

Weimer, R.J., 1984, "Relation of unconformities, tectonics, and sea-level changes, Cretaceous of western interior, U.S.A., in Schlee, J.S., eds., Interregional unconformities and hydrocarbon accumulation": AAPG Memoir v. 36, p. 7-35.

White, J.E., 1982, "Computed waveforms in transversely isotropic media": Geophysics, v. 47, p. 771-783.

White, J.E., Martineau-Nicoletis, L. and Monash, C., 1983, Measured anisotropy in Pierre Shale: Geophys. Prosp., v. 31, p. 709-725.

Wright, J., 1987, "The effects of transverse isotropy on reflection amplitude versus offset": Geophysics, v. 52, p. 564-567.

Wyllie, M.R.J., Garder, G.H.F. and Gregory, A.R.: "Studies of Elastic Wave attenuation in porous media," paper presented at 31st annual meeting of SEG (Nov. 5-9, 1961).

Young, G.B. and L.W. Braile, 1976, "A computer program for the application of Zoeppritz's amplitude equations and Knott's energy equations": Bulletin of the Seismological Society of America, v. 66, p. 1881-1885.

Zoeppritz, K., 1919, VIIb: Über reflexion und Durchgang seismischer wellen durch Unstitigkeitsflachen: Gottinger Nachrichten, p. 66-84.

## APPENDIX A

### Acquisition Parameters

Recorded by: CGG crew 512
Date recorded: 10/1/85 - 10/6/85
Recording system: Sercel SN348
Sample rate: 4 ms
Record length: 6 sec
Low cut filter: out
High cut filter: 62.5 hz
Slope: 72 db/oct
Notch: out

Near offset: 412.5 ft
Far offset: 13612.5 ft
Number of group: 80
Group interval: 165 ft

Energy source: Vibroseis* 3 Mertz Model 18
Source array: 330 ft
Number of Vibs/up: 3
Number of sweeps/up: 9
Sweep frequency: 8 - 64 hz
Sweep length: 12 sec

Geophone type: Geosource, GS20DX
Geophone frequency: 14 hz
Number per group: 24

From Martin (1987)

* Trademark of Continental Oil Corp.

# APPENDIX B

## Core Sample Measurements

| | |
|---|---|
| Well site: | Golden Buckeye Champlin #9-1<br>NWNE, Sec. 9, T15N, R64W |
| Depth range of core: | 7925 - 7985 ft |
| Rock type: | Shaly limestone with thin layers of shale, occasionally with thin layers of shell fossil. |
| Color: | Dark grey (thin layer shale).<br>Grey to dark grey (shaly limestone).<br>White grey (relatively pure limestone).<br>White (fossil layer). |
| Structure: | Horizontal layer.<br>Vertical and horizontal joint (clevage), change of mineral or rock type face (limestone, shale). |
| Environment: | Horizontal sedimentation (horizontal layers of fossitl). |
| Measurements: | Length of sample: 2.816 inch.<br>Diameter of sample: 1.000 inch.<br>Dry weight: 90.106 gram.<br>Wet weight: 91.131 gram.<br>Jolly Weight: 54.604 gram.<br>Porosity: 2.8%<br>Matrix density: 2.57 g/cm$^3$.<br>Bulk density: 2.50 g/cm$^3$.<br>Bulk volume: 36.2 cm$^3$ |

APPENDIX B
(Continued)

Velocity Measurements:

Dry sample:

| PC (Psi) | PP (Psi) | Tp (μs/ft) | Ts (μs/ft) | Vp (ft/s) | Vs (ft/s) | Poisson's Ratio |
|---|---|---|---|---|---|---|
| 1000 | 0 | 26.76 | 47.17 | 16284 | 9319 | 0.26 |
| 3000 | 0 | 26.08 | 46.44 | 16073 | 9301 | 0.25 |
| 4560 | 0 | 25.97 | 46.40 | 15953 | 9286 | 0.24 |
| 6000 | 0 | 25.78 | 46.35 | 15248 | 9025 | 0.23 |

Wet Sample:

| PC (Psi) | PP (Psi) | Tp (μs/ft) | Ts (μs/ft) | Vp (ft/s) | Vs (ft/s) | Poisson's Ratio |
|---|---|---|---|---|---|---|
| 1000 | 0 | 26.27 | 48.20 | 15749 | 8682 | 0.28 |
| 3000 | 0 | 25.93 | 47.67 | 16117 | 8855 | 0.29 |
| 4560 | 0 | 25.78 | 47.28 | 16285 | 8988 | 0.28 |
| 6000 | 0 | 25.66 | 47.17 | 16422 | 9026 | 0.29 |

# APPENDIX C

## Model From Velocity Logs

| Layer | Depth (top) | Density (g/cm$^3$) | Vp (ft/s) | Vs (ft/s) | Poisson's Ratio |
|---|---|---|---|---|---|
| 1 | 0 | 2.03 | 6045 | 2558 | 0.391 |
| 2 | 1500 | 2.20 | 8320 | 3670 | 0.379 |
| 3 | 2010 | 2.23 | 8772 | 4084 | 0.362 |
| 4 | 2400 | 2.29 | 9824 | 4565 | 0.362 |
| 5 | 3150 | 2.28 | 9667 | 3958 | 0.399 |
| 6 | 3600 | 2.31 | 10162 | 4988 | 0.341 |
| 7 | 4122 | 2.36 | 11151 | 5441 | 0.344 |
| 8 | 4275 | 2.31 | 10121 | 5079 | 0.332 |
| 9 | 4975 | 2.37 | 11239 | 5958 | 0.305 |
| 10 | 5415 | 2.34 | 10728 | 5360 | 0.333 |
| 11 | 5633 | 2.41 | 12137 | 5956 | 0.341 |
| 12 | 6080 | 2.34 | 10763 | 5465 | 0.327 |
| 13 | 6468 | 2.29 | 9790 | 4937 | 0.329 |
| 14 | 6585 | 2.36 | 11073 | 5926 | 0.300 |
| 15 | 6745 | 2.33 | 10471 | 5130 | 0.342 |
| 16 | 6875 | 2.39 | 11716 | 5910 | 0.329 |
| 17 | 7730 | 2.33 | 10475 | 5135 | 0.342 |
| 18 | 7920 | 2.46 | 13060 | 7172 | 0.284 |
| 19 | 8060 | 2.41 | 11984 | 6481 | 0.294 |
| 20 | 8137 | 2.47 | 13178 | 7197 | 0.287 |

From O'Rourke (1986)

APPENDIX D

# 7 Layer Model

**Depth (ft.)**

| | | | |
|---|---|---|---|
| 0 | | | |
| | P=5860 | $S_1$=2520 | $S_2$=2330 |
| 1000 | | | |
| | P=6720 | $S_1$=3130 | $S_2$=2900 |
| 2000 | | | |
| | P=6060 | $S_1$=2920 | $S_2$=2700 |
| 2105 | | | |
| | P=10810 | $S_V$=5460 | $S_H$=5200 |
| 5325 | | | |
| | P=11290 | $S_V$=5920 | $S_H$=5640 |
| 6700 | | | |
| | P=11680 | $S_V$=6090 | $S_H$=5800 |
| 8110 | | | |
| | P=13220 | $S_V$=7540 | $S_H$=7180 |
| 9000 | | | |
| | P=11110 | $S_V$=5500 | $S_H$=5240 |

**AZIMUTHAL ANISOTROPY**
$S_1$ = N45°W
$S_2$ = N45°E
$S_1$ = 1.08 x $S_2$

**TRANSVERSE ISOTROPY**
$S_V$ = E—W
$S_H$ = N—S
$S_V$ = 1.05 $S_H$

All velocities in ft/sec

**From Cameron**